



Fear learning induces $\alpha 7$ -nicotinic acetylcholine receptor-mediated astrocytic responsiveness that is required for memory persistence

Kuan Zhang^{1,10}, Rita Förster^{2,3,10}, Wenjing He¹, Xiang Liao⁴, Jin Li¹, Chuanyan Yang¹, Han Qin⁴, Meng Wang¹, Ran Ding¹, Ruijie Li^{1,5}, Tingliang Jian¹, Yanhong Wang¹, Jianxiong Zhang¹, Zhiqi Yang¹, Wenjun Jin¹, Yonghai Zhang^{2,3}, Song Qin⁶, Yacheng Lu⁷, Tao Chen^{7,8}, Jillian Stobart⁹, Bruno Weber⁹, Helmuth Adelsberger^{2,3}, Arthur Konnerth^{1,2,3} and Xiaowei Chen^{1,2}

Memory persistence is a fundamental cognitive process for guiding behaviors and is considered to rely mostly on neuronal and synaptic plasticity. Whether and how astrocytes contribute to memory persistence is largely unknown. Here, by using two-photon Ca^{2+} imaging in head-fixed mice and fiber photometry in freely moving mice, we show that aversive sensory stimulation activates $\alpha 7$ -nicotinic acetylcholine receptors (nAChRs) in a subpopulation of astrocytes in the auditory cortex. We demonstrate that fear learning causes the de novo induction of sound-evoked Ca^{2+} transients in these astrocytes. The astrocytic responsiveness persisted over days along with fear memory and disappeared in animals that underwent extinction of learned freezing behavior. Conditional genetic deletion of $\alpha 7$ -nAChRs in astrocytes significantly impaired fear memory persistence. We conclude that learning-acquired, $\alpha 7$ -nAChR-dependent astrocytic responsiveness is an integral part of the cellular substrate underlying memory persistence.

Memory persistence, or remembering, refers to a systematic process of making information permanently stored and cataloged in the brain so that it can be retrieved on request¹. This fundamental cognitive process plays a central role in guiding behaviors that are essential for survival² and is often impaired in neurological disorders such as Alzheimer's disease or traumatic brain injury³. Previous studies have focused extensively on the role of neurons in memory persistence. It has been suggested that memory persistence involves the replay of the neuronal activity pattern that is present at encoding^{4,5}. To increase the probability that the specific activity pattern reemerges later, memory persistence requires the strengthening or weakening of the synaptic connectivity within participating neuronal ensembles^{4,6}. Therefore, any factors that can change the synaptic connectivity strength of particular neuronal networks may affect memory persistence¹.

Accumulating experimental evidence indicates that glial cells are significant regulators of synaptic function and plasticity^{7,8}. Astrocytes, a major class of glial cells, respond to neuronal activity with intracellular Ca^{2+} transients and then release gliotransmitters that in turn modify synaptic connectivity⁸. Such mutual neuron–astrocyte interactions lead to the concept of the ‘tripartite synapse’, where astrocytes are considered as being active participants in synaptic processing⁸. Astrocytes express different types of neurotransmitter receptors, including noradrenergic, glutamatergic and cholinergic receptors⁹. Through these receptors, astrocytes

in the central nervous system respond to various sensory stimuli, including smell, light, sound, tactility and pain^{10–13}. These astrocytic signals not only modulate synapse formation, transmission and plasticity^{8,14,15} but also regulate the synchronization of neuronal population activity¹⁶. Thus, through multiscale regulation of neuronal activity during external sensory stimulation, astrocytes are in an ideal position for contributing to memory formation and persistence^{8,17}.

Indeed, astrocytes have been repeatedly shown to be involved in neuronal plasticity both in vitro^{14,15} and in vivo^{13,18}. Furthermore, a growing body of studies has revealed the necessity of astrocytes for normal memory functions in vivo^{19–22}. These studies showed that interfering with astrocytic activity results in memory impairments. In addition, recent studies showed that adding human astrocytes to the mouse brain²³ or artificially activating astrocytes²⁴ can cause memory enhancement. However, it is unknown whether and how memory-related astrocytic activity changes during information acquisition and storage, because of difficulties in identifying functionally defined astrocytes in vivo and monitoring their activity in behaving animals across different learning stages over many days. Such investigations would identify the cellular substrate by which astrocytes interact with neurons and contribute to memory formation and persistence.

Fear memory can remain intact for the entire lifetime⁵. Recent studies indicated that astrocytes contribute to the initial stages of

¹Brain Research Center and State Key Laboratory of Trauma, Burns, and Combined Injury, Third Military Medical University, Chongqing, China. ²Institute of Neuroscience, Technical University of Munich, Munich, Germany. ³Munich Cluster for Systems Neurology (SyNergy) and Center for Integrated Protein Sciences, Munich, Germany. ⁴Center for Neurointelligence, School of Medicine, Chongqing University, Chongqing, China. ⁵Advanced Institute for Brain and Intelligence, Guangxi University, Nanning, China. ⁶Department of Anatomy Histology and Embryology, Shanghai Medical College, Fudan University, Shanghai, China. ⁷Department of Anatomy Histology & Embryology, Air Force Medical University, Xi'an, China. ⁸Center for Neuron and Disease, Frontier Institute of Science and Technology, Xi'an Jiaotong University, Xi'an, China. ⁹Institute of Pharmacology and Toxicology, University of Zurich and Neuroscience Center Zurich, Eidgenössische Technische Hochschule, Zurich, Switzerland. ¹⁰These authors contributed equally: Kuan Zhang, Rita Förster. ✉e-mail: arthur.konnerth@tum.de; xiaowei_chen@tmmu.edu.cn

fear memory acquisition and consolidation^{19–22,24}. The artificial activation of astrocytes by chemogenetic manipulations in the CA1 region of the hippocampus can enhance fear memory acquisition²⁴ but may reduce fear expression in the medial subdivision of the central amygdala²⁰. In addition, in the auditory cortex, fear learning has been shown to involve neuronal plasticity^{25,26} and depend on the recruitment of $\alpha 7$ -nAChR-mediated activation of disinhibitory neuronal circuits^{26,27}. However, it is unknown whether astrocytes in the auditory cortex are involved in the process of fear memory formation and persistence.

In this study, we interrogated the role of cortical astrocytes in memory formation and persistence by using two-photon Ca^{2+} imaging in head-fixed mice^{9,28}, optical fiber-based recording in freely moving mice^{29,30} and astrocyte-specific ablation of $\alpha 7$ -nAChRs in an auditory associative fear learning task. We discovered a de novo-induced astrocytic responsiveness mediated by sensory stimulation-activated $\alpha 7$ -nAChRs in the auditory cortex during fear memory formation. This responsiveness persisted along with the fear memory behavior over days and ended with its experimentally induced extinction. Specifically, blocking this astrocytic responsiveness impaired memory persistence. Therefore, we suggest that $\alpha 7$ -nAChR-activated astrocytes in the mammalian auditory cortex are essential for the persistence of fear memory.

Results

Footshock activates astrocytes in the auditory cortex. We started our study by determining the activity patterns of astrocytes in layers 1 (L1) and 2/3 (L2/3) of the auditory cortex stained with the Ca^{2+} indicator Fluo-8 acetoxymethyl ester (Fluo-8 AM) by using a bulk-loading approach^{9,28} (Fig. 1a and Supplementary Fig. 1a). With our adapted protocol (Methods), effective astrocytic labeling with Fluo-8 AM was obtained in a larger region of the auditory cortex, including the primary auditory cortex, the ventral secondary auditory cortex and part of the adjacent temporal association cortex. The specificity of astrocyte labeling with Fluo-8 AM was confirmed by additional sulforhodamine 101 staining³¹ (Supplementary Fig. 1b). Figure 1a,b illustrates an experiment in which we monitored the activity of astrocytes within a field of view while delivering either sound stimuli or footshocks to a hind limb. We first used recording conditions of light anesthesia (<0.5% isoflurane) that did not cause the blockade of astrocytic Ca^{2+} signals observed at deeper levels of anesthesia^{12,32}. Surprisingly, while in this experiment none of the astrocytes tested responded to sound stimulation, four out of eight astrocytes reliably responded with Ca^{2+} transients to footshock stimulation ('responders'). Results obtained from similar experiments in 15 animals (189 cells) confirmed these observations by showing that a large fraction of astrocytes was responsive to footshock but only a minority to sound stimulation (details below). To further verify these results with a sensor suited to longitudinal experiments, we expressed the genetically encoded Ca^{2+} indicator GCaMP6s³³ specifically in astrocytes of the auditory cortex by

injecting the adeno-associated virus (AAV)–serum glial fibrillary acidic protein (sGFAP)–GCaMP6s construct^{34,35}. Figure 1c,d indicates that GCaMP6s-stained astrocytes had a similar response pattern to those stained with Fluo-8 AM. Across all recordings obtained with these two Ca^{2+} sensors, about 64% of astrocytes (a total of 328 cells in 25 animals tested consisting of 189 cells per 15 mice for Fluo-8 AM and 139 cells per 10 mice for GCaMP6s) reliably responded with Ca^{2+} transients to footshock stimulation, while only 8% responded to sound stimulation (Fig. 1e; see the example of sound-evoked astrocytic responses in Extended Data Fig. 1). As a caveat, we have no direct confirmation on the status of neuronal activity. Nevertheless, we stress that similar sound stimulation is well known to effectively activate large groups of neurons in the auditory cortex^{36–40}. The footshock-evoked astrocytic Ca^{2+} transients occurred at a relatively large range of latencies after the stimulus (Fig. 1f), similarly to sensory stimulation-evoked astrocytic responses detected in other sensory cortex regions^{11,12}. Footshock-evoked astrocytic responses were not restricted to the auditory cortex but were observed in other cortical regions, for example, in the somatosensory cortex (Supplementary Fig. 2). Together, these results establish that footshock, but not sound, represents a reliable stimulus for the activation of cortical astrocytes.

Multiple lines of evidence from in vitro and in vivo studies indicate that astrocytic Ca^{2+} transients are often mediated by the activation of G_q -coupled neurotransmitter receptor-driven Ca^{2+} release from intracellular endoplasmic reticulum Ca^{2+} stores^{18,41}. Consistent with those earlier observations, we found that footshock-evoked Ca^{2+} transients were suppressed by the sarco/endoplasmic reticulum Ca^{2+} -ATPase antagonist cyclopiazonic acid (CPA) (Fig. 1g,h) or thapsigargin (Fig. 1h and Extended Data Fig. 2a), both known to deplete endoplasmic reticulum Ca^{2+} stores. Furthermore, application of ryanodine (Fig. 1h and Extended Data Fig. 2b) largely suppressed footshock-evoked responses, indicating an involvement of ryanodine receptors⁴¹. As demonstrated in several previous studies^{9,12,13,32,42–44}, such astrocytic Ca^{2+} -induced Ca^{2+} release signals recorded in cell bodies occurred at relatively long latencies after sensory stimulation (Fig. 1f), in contrast to the short latency signals that can be recorded at the more remote microdomains of the astrocytic processes, the presumed sites of synaptic interaction³⁴. Anesthesia was not a relevant determinant for the prolonged delays (anesthetized mice, 3.1 ± 0.2 s, $n = 5$ mice versus awake mice, 2.7 ± 0.1 s, $n = 4$ mice; $P = 0.2264$, two-sided Wilcoxon rank-sum test; Extended Data Fig. 3).

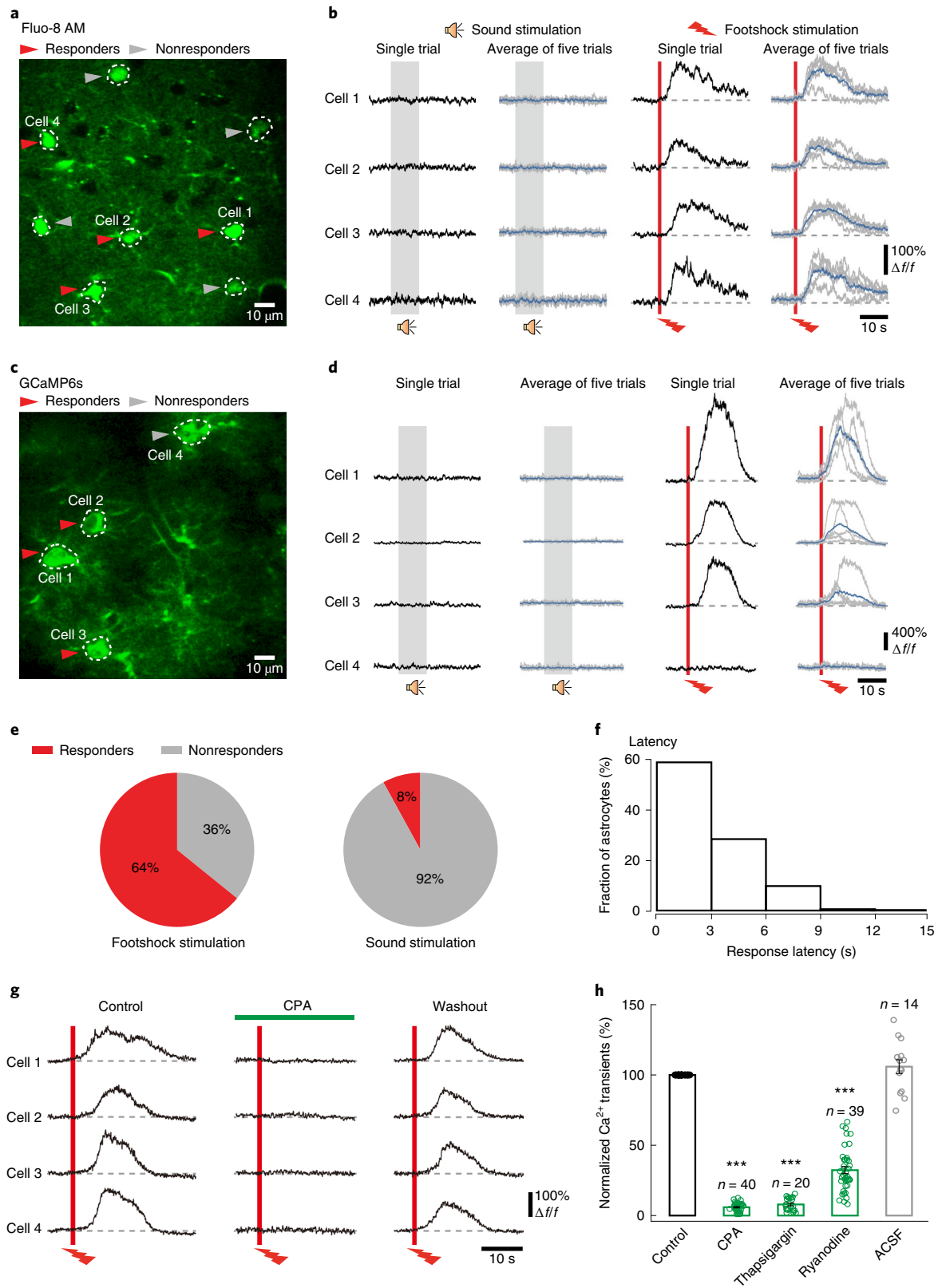
$\alpha 7$ -nAChR-mediated activation of auditory cortex astrocytes.

Unlike the spontaneous astrocytic Ca^{2+} waves in the hippocampus in vivo that require gap junction-dependent glia–glia communication⁴⁵, footshock-evoked Ca^{2+} transients were largely insensitive to the gap junction inhibitor carbenoxolone (Extended Data Fig. 2c,d; $n = 22$ cells, 4 mice). Instead, the astrocytic Ca^{2+} transients were completely abolished in 5 out of 5 experiments by the Na^+

Fig. 1 | Sensory stimulation-evoked Ca^{2+} signaling in astrocytes of the mouse auditory cortex. **a**, Two-photon fluorescence image of Fluo-8 AM-stained astrocytes in L2/3 of the mouse auditory cortex. The imaging depth was $171 \mu\text{m}$ below the cortical surface. The red arrowheads indicate astrocytes that responded to footshock stimulation ('responders'), while the gray arrowheads indicate nonresponding cells ('nonresponders'). **b**, Sound- and footshock-evoked Ca^{2+} transients ($\Delta f/f$) corresponding to the astrocytes indicated in **a** (sound stimuli indicated by the gray bars; footshock stimuli indicated by the red bars). Both single and average trials are shown. **c**, Two-photon image of GCaMP6s-stained astrocytes in the auditory cortex. Imaging depth was $150 \mu\text{m}$. **d**, Similar experimental arrangement as in **b** involving the use of GCaMP6s instead of Fluo-8 AM. **e**, Pie charts illustrating the fraction of responding and nonresponding astrocytes to footshock (left) or sound stimulation (right), respectively ($n = 328$ cells from 25 mice). **f**, Latency histogram of footshock-evoked Ca^{2+} transients ($n = 210$ cells). **g**, Footshock-evoked Ca^{2+} transients in four representative cells of an imaging plane before, during and after local application of CPA. **h**, Bar graphs summarizing the effects of CPA, thapsigargin, ryanodine or ACSF on the footshock-evoked astrocytic Ca^{2+} transients. The amplitude of the Ca^{2+} transients was normalized to the control level (value before drug administration). The number of cells tested is indicated above each bar. *** $P < 0.001$ versus control condition (control versus CPA, $z = 5.5109$, $P = 3.5694 \times 10^{-8}$; control versus thapsigargin, $z = 3.9199$, $P = 8.8575 \times 10^{-5}$; control versus ryanodine, $z = 5.4424$, $P = 5.2553 \times 10^{-8}$; control versus ACSF, $z = -1.0986$, $P = 0.2719$), two-sided Wilcoxon signed-rank test. All data are shown as the mean \pm s.e.m.

channel antagonist tetrodotoxin (TTX), which was focally applied to the tested astrocytes (Extended Data Fig. 2e–g; $n=55$ cells, 5 mice). These experiments indicate that footshock-evoked Ca^{2+} transients in the astrocytes of the auditory cortex are dependent on afferent neuronal activity, without a detectable contribution through gap-junctional activation by other astrocytes.

Since footshock stimulation is known to activate via cholinergic afferents from the basal forebrain many cortical regions, including the auditory cortex^{26,27}, we performed pharmacological manipulations with cholinergic and other receptor antagonists under visual guidance using two-photon imaging *in vivo*. The drugs tested were applied locally to the target regions in the auditory cortex using



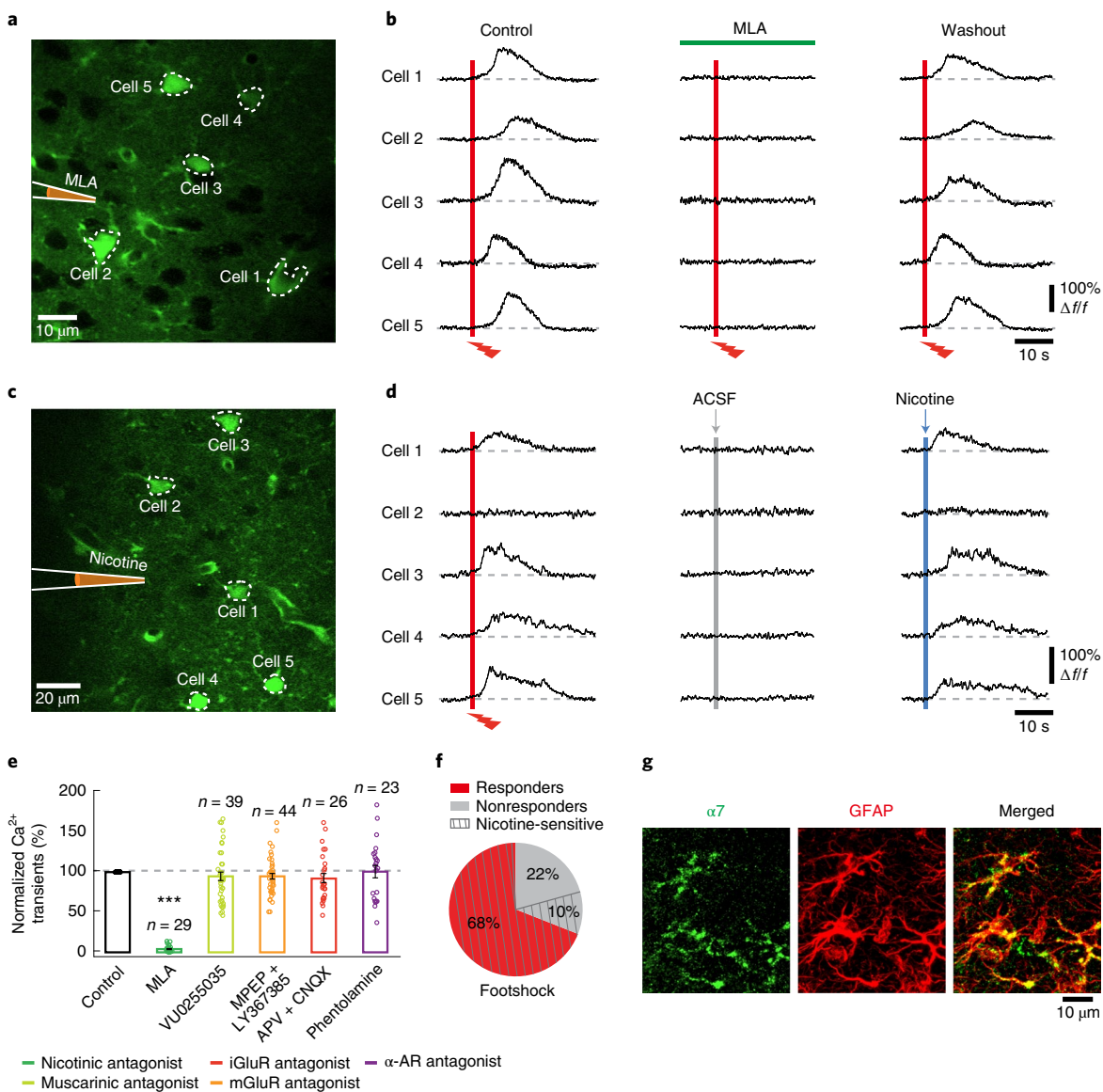


Fig. 2 | nAChR dependence of footshock-evoked astrocytic responses. **a**, Two-photon image of Fluo-8 AM-stained astrocytes with the schematic representation of the glass pipette used for local MLA application (imaging depth, 250 μm). **b**, Footshock-evoked Ca^{2+} transients obtained in the five astrocytes indicated in **a** before, during and after MLA application. **c,d**, Same arrangement as in **a,b** but through the application of ACSF or nicotine (in the presence of TTX; imaging depth, 125 μm). **e**, Bar graph summarizing the effects of MLA, VU0255035 (muscarinic AChR antagonist), combination of MPEP and LY367385 (both group I mGluR antagonists), combination of APV and CNQX (ionotropic glutamate receptor antagonists (iGluRs)) or phentolamine (α -adrenergic receptor antagonist) on footshock-evoked Ca^{2+} transients. The amplitudes of the Ca^{2+} transients were normalized to control levels (values before drug application). The number of cells is indicated above each bar. $***P < 0.001$ versus control (control versus MLA, $z = 4.7033$, $P = 2.5596 \times 10^{-6}$; control versus VU0255035, $z = 1.4374$, $P = 0.1506$; control versus MPEP + LY367385, $z = 1.87$, $P = 0.0615$; control versus APV + CNQX, $z = 1.4604$, $P = 0.1442$; control versus phentolamine, $z = 0.1521$, $P = 0.8791$), two-sided Wilcoxon signed-rank test. **f**, Pie chart illustrating the nicotine sensitivity (striped area) of cells responding (responders) or not responding (nonresponders) to footshock ($n = 69$ cells). **g**, Confocal images of a cortical section of the mouse auditory cortex immunostained for the $\alpha 7$ subunit (green, left) and GFAP (red, middle). Similar results were obtained in 13 slices from 3 mice. All data are shown as the mean \pm s.e.m.

glass pipettes that also contained, for better visualization, the pharmacologically inert fluorescent dye Alexa Fluor 594 (AF594) (Fig. 2a–d). We found that the nAChR antagonist methyllycaconitine (MLA) abolished completely, and fully reversibly, the Ca^{2+} transients evoked by footshock stimulation (Fig. 2a,b,e). In contrast, neither the muscarinic AChR antagonist VU0255035 (Fig. 2e and Extended Data Fig. 2h) nor a combination of the metabotropic glutamate receptor (mGluR) antagonists 2-methyl-6-(phenylethynyl)pyridine (MPEP) (mGluR5 antagonist) and LY367385 (mGluR1 antagonist;

Fig. 2e and Extended Data Fig. 2i) nor ionotropic glutamate receptor antagonists ((2R)-2-amino-5-phosphonopentanoic acid (APV) and cyanquinoxaline (CNQX)) (Fig. 2e and Extended Data Fig. 2j) were effective. Earlier studies showed that a startle response^{43,46} or a high vigilance state⁴⁷ can evoke astrocytic Ca^{2+} transients through norepinephrine-mediated activation of α -adrenergic receptors in the neocortex. However, in our recordings in the auditory cortex obtained at both awake and anesthetized states, footshock-evoked astrocytic Ca^{2+} transients were insensitive to the α -adrenergic receptor

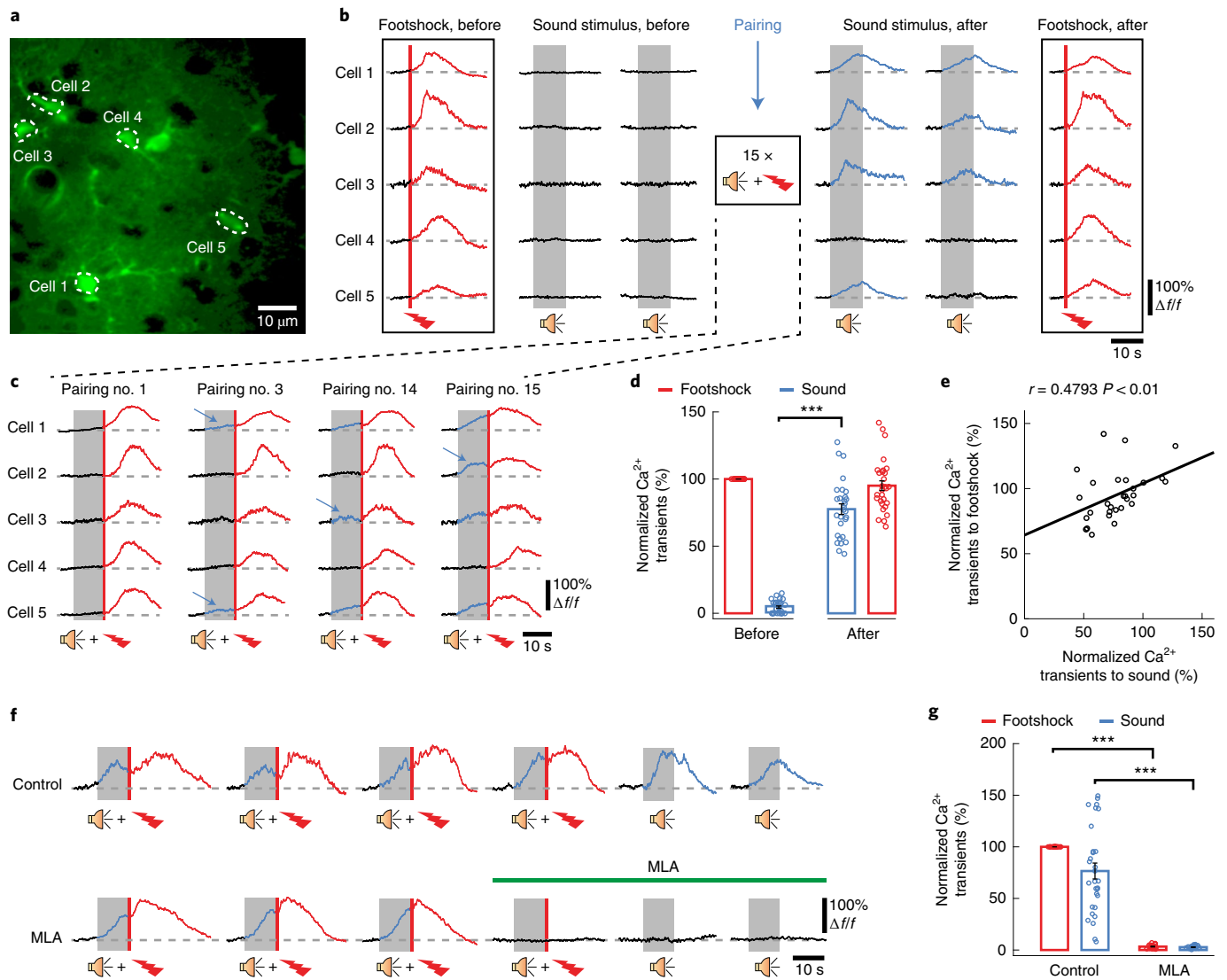


Fig. 3 | De novo induction of sound-evoked astrocytic responses by fear learning. **a**, Two-photon image of a Fluo-8 AM-stained area in the auditory cortex (imaging depth, 269 μm). **b**, Left: Ca^{2+} transients recorded in astrocytes indicated in **a** (red traces, 'footshock, before') during footshock or sound stimulation (black traces, 'sound stimulus, before'; two consecutive trials) before pairing. Right: Sound-evoked responsiveness (blue traces, 'sound stimulus, after'; two consecutive trials) and footshock-evoked responses ('footshock, after') after pairing. **c**, Ca^{2+} transients during conditioning for selected pairs of sound/footshock stimuli. Note the gradual development of responsiveness to sound stimulation (blue arrows and traces) for cells 1-3 and 5. **d**, Bar graph summarizing the changes in amplitude of astrocytic Ca^{2+} transients in response to sound (blue) or footshock (red) stimulation before and after conditioning. All amplitudes were normalized to that of the respective initial Ca^{2+} transients produced by footshock (fear conditioning; $n=29$ cells from 4 mice; before versus after footshock, $z=1.7306$, $P=0.0835$; before versus after sound, $z=-4.7030$, $P=2.5631 \times 10^{-6}$; $***P < 0.001$, two-sided Wilcoxon signed-rank test). **e**, Plot of sound- versus footshock-evoked astrocytic Ca^{2+} transient amplitudes after conditioning. $n=29$ cells from 4 mice, Spearman $r=0.4793$, two-tailed $P=0.0092$, $P < 0.01$. **f**, MLA-dependent blockade of footshock- and sound-evoked responses. The duration of MLA application is indicated by a green bar. **g**, Bar graph summarizing MLA blockade. The amplitudes of the Ca^{2+} transients were normalized to those of the initial footshock-evoked responses ($n=28$ cells from 4 mice; control-footshock versus MLA-footshock, $z=4.6227$, $P=3.7869 \times 10^{-6}$; control-sound versus MLA-sound, $z=-4.6226$, $P=3.7896 \times 10^{-6}$; $***P < 0.001$, two-sided Wilcoxon signed-rank test). All data are shown as the mean \pm s.e.m.

antagonist phentolamine (Fig. 2e and Extended Data Fig. 4a,b) or the $\alpha 1$ -adrenergic receptor antagonist prazosin (Extended Data Fig. 4c,d). These findings are in clear contrast to the antagonistic effects of these drugs on startle responses or on vigilance states^{43,46,47}.

The specific role of nAChRs was further substantiated by the observation that all astrocytes that responded to footshock stimulation ('responders') also responded with Ca^{2+} transients to directly applied nicotine (delivered in the presence of TTX to prevent contributions of nearby neurons, $n=69$ cells tested; Fig. 2c,d,f). Furthermore, these astrocytes expressed $\alpha 7$ -nAChRs (Extended Data Fig. 5). Instead, most 'nonresponders' could not be activated

by nicotine (Fig. 2f). Finally, we used immunostaining to demonstrate the presence of nAChR $\alpha 7$ subunit-specific puncta on GFAP-positive processes of auditory cortex astrocytes (Fig. 2g)⁹.

Fear learning-induced astrocytic responsiveness to sound. To investigate whether fear learning has any impact on the activity of astrocytes, we next performed in vivo two-photon Ca^{2+} imaging experiments in head-fixed, lightly anesthetized mice before, during and after the presentation of conditioning paired tone/footshock stimuli. After screening different pure tone and complex sound stimulation patterns, known to be differently effective in different

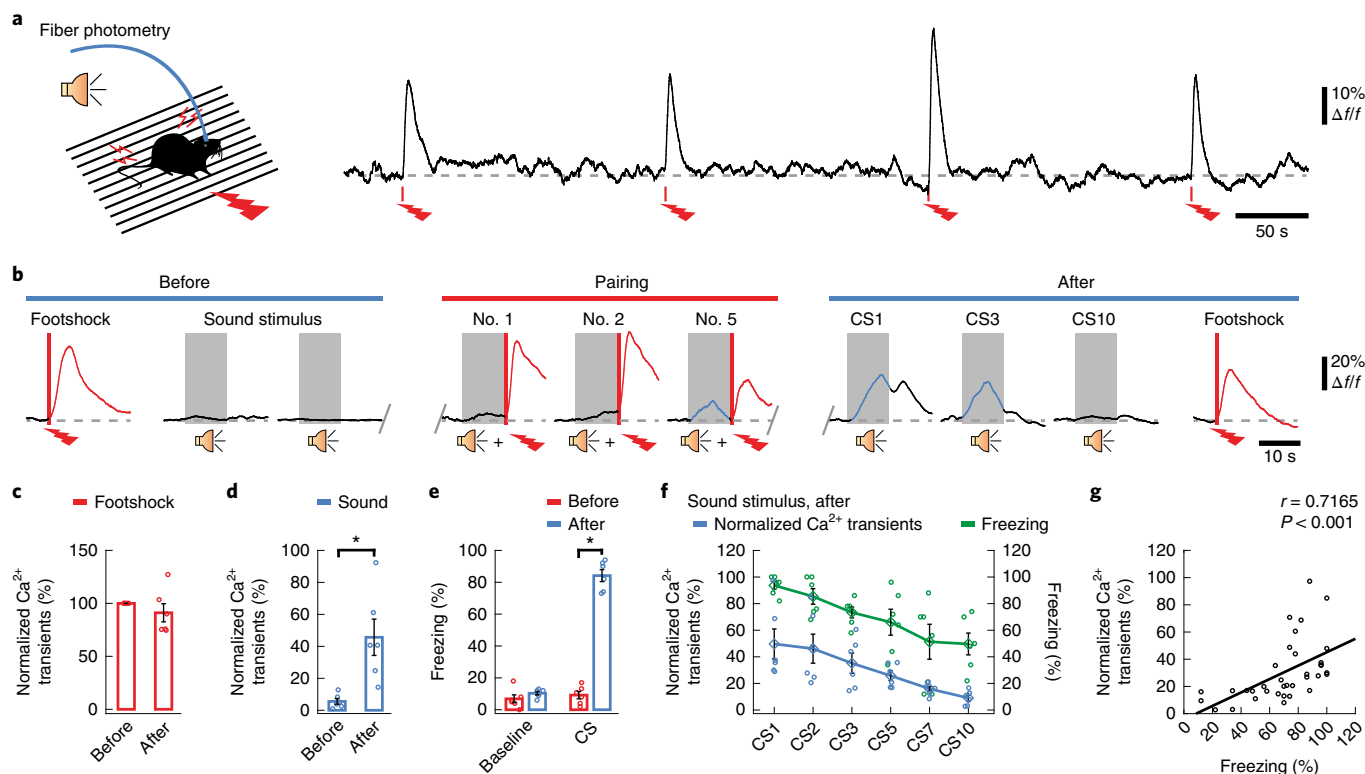


Fig. 4 | Fear learning-dependent induction of astrocytic Ca^{2+} responsiveness in awake behaving mice. **a**, Recording of astrocytic Ca^{2+} signals in freely moving mice by fiber photometry. Left: Schematic of the optical fiber recording. Right: Footshock-evoked astrocytic Ca^{2+} transients during consecutive trials. **b**, Astrocytic Ca^{2+} transients in response to footshock or sound before, during and after pairing. **c,d**, Bar graphs summarizing the amplitudes of astrocytic Ca^{2+} transients in response to footshock (**c**) or sound (**d**) before and after conditioning. $n=6$ mice in each group (**c**, ‘footshock-before’ versus ‘footshock-after’, $z=0.7338$, $P=0.4631$; **d**, ‘sound-before’ versus ‘sound-after’, $z=-2.2014$, $P=0.0277$; $*P<0.05$, two-sided Wilcoxon signed-rank test). **e**, Summary of freezing levels before and after conditioning. $n=6$ mice (baseline: before versus after, $z=-0.9540$, $P=0.3401$; CS: before versus after, $z=-2.2014$, $P=0.0277$; $*P<0.05$, two-sided Wilcoxon signed-rank test). **f**, Summary of the decline of astrocytic Ca^{2+} responsiveness (blue) and freezing levels (green) over multiple sound stimuli after conditioning ($n=6$ mice). **g**, Correlation between amplitudes of astrocytic Ca^{2+} transients and freezing levels in response to sound after conditioning. $n=36$ trials from 6 mice; Spearman $r=0.7165$, two-tailed $P=8.9087 \times 10^{-7}$, $P<0.001$. All data are shown as the mean \pm s.e.m.

auditory cortex subregions^{25,27,40}, we identified a pure tone stimulation protocol (Methods) as being the most effective under our experimental conditions. Also, instead of the standard protocol of 3–5 tone/footshock pairings used in unanesthetized animals^{5,27}, in lightly anaesthetized animals we needed 10–15 pairings to induce long-lasting fear memory. We confirmed that this protocol was indeed effective by showing that the freezing behavior tested during wakefulness was similar, in terms of strength and persistence, to that observed after conditioning in freely moving animals (Fig. 6b versus Supplementary Fig. 6).

In the experiment illustrated in Fig. 3a–c, we show the changes in five astrocytes that initially produced Ca^{2+} transients in response to pure footshock but not in response to pure sound stimuli (Fig. 3b, columns preceding pairing showing one footshock trial and two consecutive sound trials). Figure 3c illustrates the changes in the Ca^{2+} signaling pattern when delivering repetitively paired stimuli at an interval of 3 min. While pairing no. 1 evoked a pure footshock-evoked response, we observed already with pairing no. 3 a trend of astrocytic responsiveness to sound stimuli indicated by the slight upward deflections in the Ca^{2+} trace of cell 1 and cell 5 (blue arrows in Fig. 3c). In the next 15 pairings, cells 1, 2, 3 and 5, but not cell 4, developed bona fide sound-evoked Ca^{2+} transients. At the end of the pairing period, Ca^{2+} transients could be evoked just by sound stimuli alone (Fig. 3b, columns after pairing showing two consecutive sound trials and one footshock trial). Similar observations were

made in 30 out of 30 astrocytes tested (4 mice; Fig. 3d). Trace fear conditioning stimulation, involving hippocampal-dependent processes⁴⁸, was ineffective in inducing astrocytic sound-evoked Ca^{2+} responsiveness (Extended Data Fig. 6). Despite multiple control and conditioning stimuli in ongoing experiments, the amplitudes of footshock-evoked Ca^{2+} transients did not change during repeated stimulation (Fig. 3b, last column and Fig. 3d). Remarkably, while there was a highly significant increase in the number of astrocytes with de novo-induced sound-evoked responsiveness, the number of astrocytes responding to footshock stimulation was constant. Furthermore, sound responsiveness was acquired only in those astrocytes (‘responders’: approximately 68% versus 5% before conditioning, $n=30$ cells, 4 mice) that were footshock-responsive but not in ‘nonresponders’. Notably, the response amplitudes to sound stimulation after conditioning correlated positively with the corresponding footshock-evoked responses (Fig. 3e), suggesting that an overlapping set of afferent axons underlie the newly induced astrocytic Ca^{2+} responses.

To explore the contribution of cholinergic inputs to the learned astrocytic responsiveness to sound stimulation, we applied the nAChR antagonist MLA locally and found that it abolished both footshock- and sound-induced astrocytic Ca^{2+} transients (Fig. 3f). Such a blockage effect was observed in 28 out of 28 astrocytes tested in 4 mice (Fig. 3g). Supplementary Fig. 3 shows that the MLA block was fully reversible. We conclude that nAChR-dependent activation

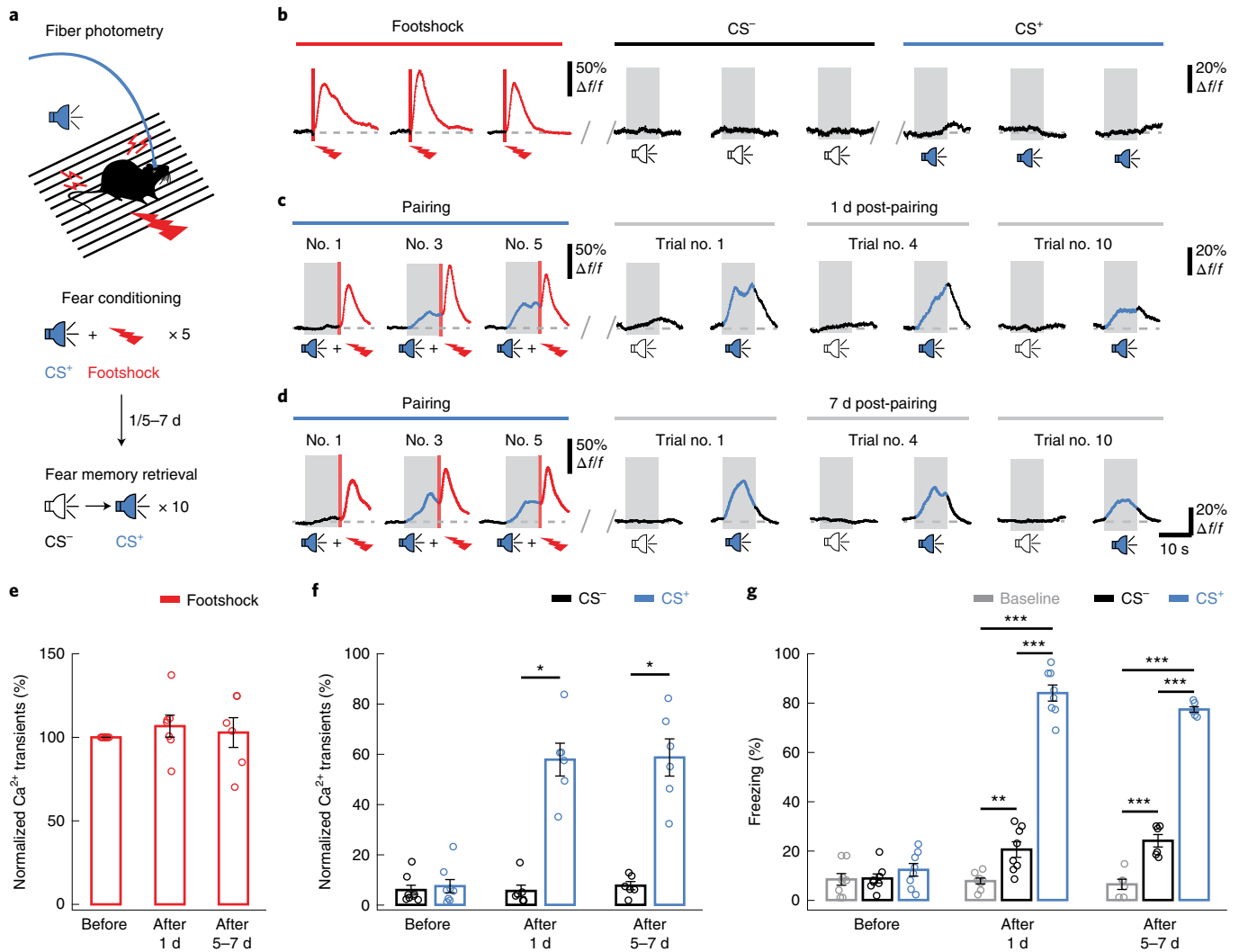


Fig. 5 | De novo induction of sound-evoked astrocytic Ca²⁺ responses by CS⁺ but not CS⁻ in freely moving mice. **a**, Top: Schematic of optical fiber recording. Bottom: Fear conditioning protocol. **b**, Ca²⁺ transients recorded in astrocytes responsive initially to footshock (red traces, first column) but not to CS⁻ or CS⁺. **c,d**, Astrocytic Ca²⁺ transients in response to footshock (e) or CS⁺/CS⁻ (f) before and 1 and 5–7 d after conditioning. **e**, Bar graphs summarizing the amplitudes of astrocytic Ca²⁺ transients in response to footshock (e) or CS⁺/CS⁻ (f) before and 1 and 5–7 d after conditioning. Footshock: $n = 8$ mice in the 'before' group, $n = 7$ mice in the 'after 1 d' group, $n = 6$ mice in the 'after 5–7 d' group (e: 'footshock before' versus 'footshock after 1 d', $z = 1.0142$, $P = 0.3105$; 'footshock before' versus 'footshock after 5–7 d', $z = 0.3145$, $P = 0.7532$); CS⁻/CS⁺: $n = 8$ mice in the 'before' group, $n = 6$ mice in the 'after 1 d' and 'after 5–7 d' group (f: 'CS⁻ before' versus 'CS⁺ before', $z = -1.4003$, $P = 0.1614$, 'CS⁻ after 1 d' versus 'CS⁺ after 1 d', $z = -2.2014$, $P = 0.0277$; 'CS⁻ after 5–7 d' versus 'CS⁺ after 5–7 d', $z = -2.2014$, $P = 0.0277$; * $P < 0.05$, two-sided Wilcoxon signed-rank test). **g**, Summary of the freezing levels to CS⁻ and CS⁺. $n = 8$ mice in the 'before' and 'after 1 d' group, $n = 6$ mice in the 'after 5–7 d' group (two-way ANOVA; main effect of condition: $F_{2,57} = 353.71$, $P = 7.37 \times 10^{-33}$; main effect of day: $F_{2,57} = 128.58$, $P = 7.48 \times 10^{-22}$; condition × day interaction: $F_{4,57} = 81.64$, $P = 6.40 \times 10^{-23}$; 'baseline after 1 d' versus 'CS⁻ after 1 d': $P = 0.0095$, 'baseline after 1 d' versus 'CS⁺ after 1 d': $P = 3.69 \times 10^{-29}$, 'CS⁻ after 1 d' versus 'CS⁺ after 1 d': $P = 4.02 \times 10^{-25}$, 'baseline after 5–7 d' versus 'CS⁻ after 5–7 d': $P = 0.0007$, 'baseline after 5–7 d' versus 'CS⁺ after 5–7 d': $P = 2.02 \times 10^{-24}$, 'CS⁻ after 5–7 d' versus 'CS⁺ after 5–7 d': $P = 1.40 \times 10^{-18}$; ** $P < 0.01$, *** $P < 0.001$, two-way ANOVA with Bonferroni post hoc comparison test). All data are shown as the mean ± s.e.m.

is of critical importance for the new, paired stimulation-dependent activity in astrocytes.

To exclude the possible effects of anesthesia, we next performed a new line of experiments entirely in awake behaving mice. For this purpose, we used an optic fiber photometer^{29,30} and implanted chronically the recording tip of a fine optic fiber into the right auditory cortex after AAV-mediated, astrocyte-specific GCaMP6f staining (Fig. 4a, left). This arrangement allowed Ca²⁺ recordings that reflected the activity of a small local cluster of stained cells that were located just in front of the tip of the optic fiber, as established previously by combined two-photon imaging and optical fiber recordings in the same experiment⁴⁹. Post hoc immunostaining

confirmed the specificity of GCaMP6f targeting to astrocytes and indicated the location of the recording sites in the auditory cortex (Supplementary Fig. 4). Fig. 4a (right) shows an example recording where repeated footshock stimuli reliably evoked astrocytic Ca²⁺ transients with comparable amplitudes. This contrasts with repetitive vigilance state-induced astrocytic Ca²⁺ responses that were shown to attenuate rapidly during consecutive stimuli⁴⁷. Figure 4b presents an example recording performed in the auditory cortex before, during and after the presentation of conditioning paired tone/footshock stimuli. In this wakefulness condition, the conditioning stimulation consisted of 3–5 tone/footshock pairings^{5,27}. The population recordings obtained from a small cluster of stained

astrocytes in awake behaving animals (Fig. 4a–g) were strikingly similar to those obtained from single astrocytes by two-photon imaging in head-fixed animals (Fig. 3a–g). Again, we observed a de novo induction of sound-evoked astrocytic Ca^{2+} responsiveness associated with fear learning (Fig. 4b,d,e). Remarkably, we observed an induction of sound-evoked astrocytic Ca^{2+} transients after fear conditioning not only in the auditory cortex but also in the hippocampus (CA1 and dorsal hippocampus; Extended Data Fig. 7) and in the basolateral amygdala (BLA) (Extended Data Fig. 8a–d) but not in the somatosensory cortex (Extended Data Fig. 8e–h). Thus, fear learning-dependent induction of astrocytic Ca^{2+} responsiveness was not restricted to the auditory cortex but also expressed in those brain regions known to participate in fear learning-dependent sound processing^{5,27}. However, whether $\alpha 7$ -nAChRs are also involved in astrocytic activation in the hippocampus and BLA has not been addressed in this study and requires future investigation.

To test for the specificity of the conditioned stimulus (CS) in the standard experiments, we used a train of 8-kHz tone pulses as CS⁺ and, as a control, a train of 2-kHz tone pulses as CS⁻. Fear memory retrieval tests were performed with either CS⁻ or CS⁺ 1 or 5–7 d after fear conditioning (Fig. 5a). Consistent with the two-photon imaging results in head-fixed animals (Fig. 3b), optic fiber-recorded astrocytic Ca^{2+} transients obtained during wakefulness were also reliably induced by footshock stimulation (Figs. 4a,c and 5b) but not by sound stimulation before fear conditioning (Fig. 4b, before and Fig. 5b). Figure 5c,d illustrates representative recordings performed at 1 and 7 d after conditioning, respectively, showing that CS⁺, but not CS⁻, successfully induced persistent astrocytic Ca^{2+} responsiveness (blue traces in Fig. 5c,d). Like the results obtained under light anesthesia (Fig. 3d), the amplitudes of the footshock-evoked Ca^{2+} transients were unchanged during repeated stimulation in the awake animals also (Fig. 5e). While CS⁺ evoked a strong and persistent potentiation of astrocytic Ca^{2+} transients after fear conditioning, CS⁻ was ineffective (Fig. 5f). Fear learning-induced freezing levels were also significantly higher during CS⁺ than during CS⁻ (Fig. 5g). As an additional control, in the conditioning experiment we reversed the identity of CS⁺ and CS⁻ to 2- and 8-kHz stimulation, respectively. As expected from previous observations (for example, ref. 40), the 2-kHz tone pulses, as CS⁺, were highly effective in inducing fear learning (Supplementary Fig. 5). Thus, we conclude that the induction of sound-evoked astrocytic responsiveness was specific to the CS⁺ but not to the untrained sound stimulus (CS⁻) that, under other conditions, can cause fear generalization⁵⁰.

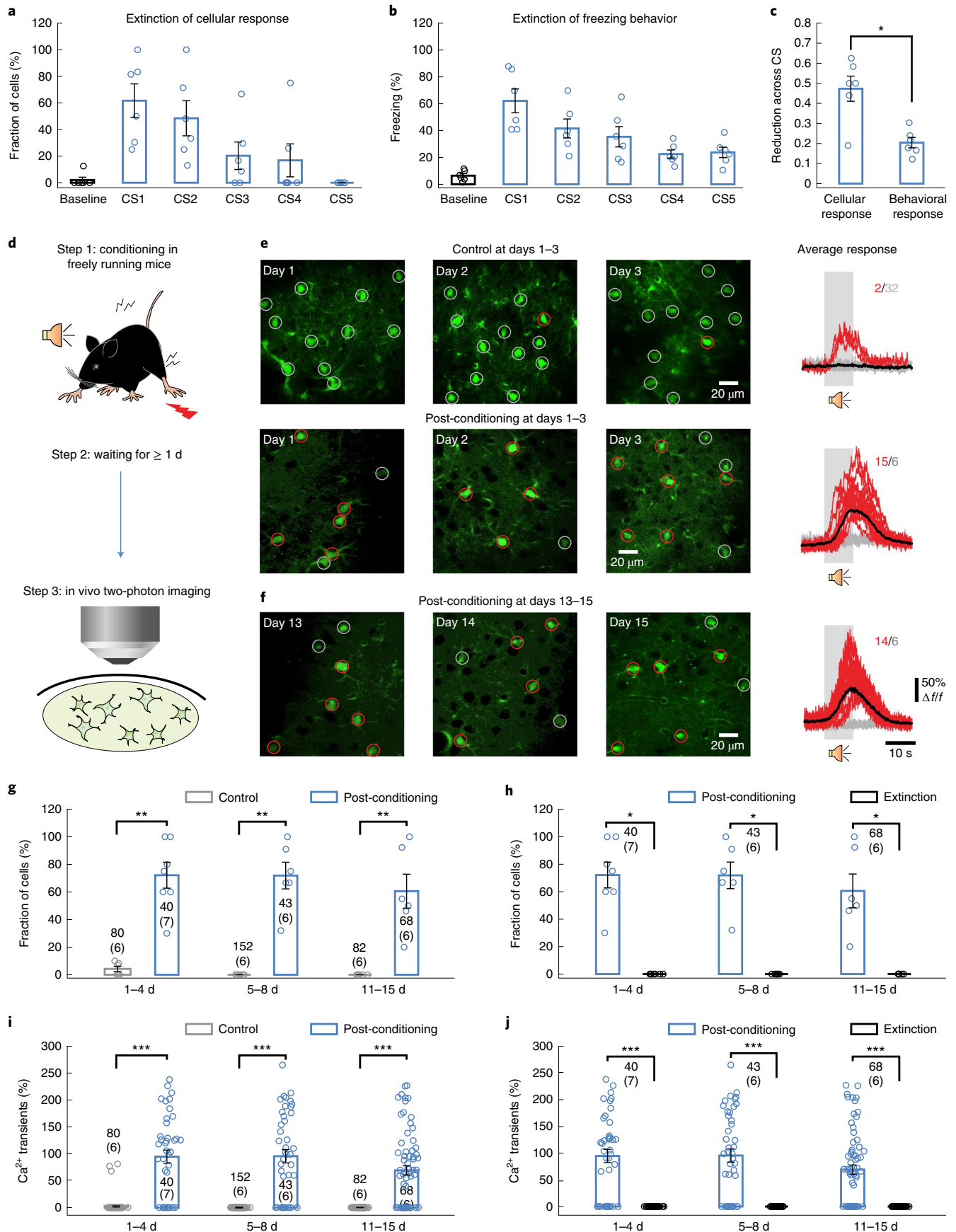
Persistence and extinction of astrocytic responsiveness. While footshock-evoked Ca^{2+} transients were extremely robust over multiple stimulation trials (for example, Figs. 3b,c, 4a and 5b), sound-evoked Ca^{2+} transients were fragile and declined during CS delivered repeatedly (Figs. 4f and 6a). Generally, after 5–10 consecutive sound stimuli, delivered at an interval of 3 min, sound-evoked astrocytic Ca^{2+} transients were virtually abolished (fiber recordings: $n = 6$ mice in Fig. 4f; two-photon imaging: $n = 80$ cells from 6 mice in Fig. 6a). Freezing levels also gradually declined over consecutive sound stimuli (Figs. 4f and 6b) and were positively correlated with the amplitudes of sound-evoked astrocytic Ca^{2+} transients (Fig. 4g), supporting the notion of a tight and direct link between astrocytic signaling and freezing behavior. Nevertheless, while the reduction (or ‘extinction’) of sound-evoked astrocytic Ca^{2+} responsiveness was nearly complete, a significant component of freezing behavior persisted ($n = 6$ mice; Figs. 4f and 6b,c)^{5,27}, indicating that the relevant neuronal circuits include astrocyte-independent signaling components.

Previous studies underscored the contribution of various types of auditory cortex neurons for fear learning and memory^{5,27}. To test the long-term correspondence between conditioned sound stimulus-activated astrocytes and fear memory, we delivered the conditioning training stimulation to awake, freely moving animals that were then tested for astrocytic Ca^{2+} signaling at cellular resolution under head-fixed conditions in the two-photon microscope (Fig. 6d). To induce fear learning in the awake state, we used 3–5 pairings and verified the effectiveness of the stimulation with behavioral tests. In control recordings, at day 0 (the day of conditioning of the test animals) naïve mice were placed without stimulation in the ‘conditioning’ box. These control animals were otherwise treated exactly like the test animals. The fraction of astrocytes responding to sound stimulation was very low before fear learning (Fig. 6e top), corresponding to what we discussed earlier (Fig. 1e). By contrast, mice that received conditioning training and were tested 1–3 d later had a very large increase in the number of sound-responding astrocytes (Fig. 6e bottom). A similar persisting increase in sound responders was observed also 13–15 d post-conditioning (Fig. 6f). Across all experiments (Fig. 6g–j), both the fraction of sound responders and their response strengths were remarkably stable over the period tested (up to 15 experimental days; Fig. 6g,i). Entirely consistent with these results, we found that the CS induced in awake behaving mice sound-evoked astrocytic Ca^{2+} transients that persisted until the active experimental extinction, for example,

Fig. 6 | Long-term persistence and extinction of astrocytic responsiveness. **a**, ‘Extinction’ of cellular responsiveness indicated by the gradual disappearance of response to sound during repeatedly delivered CS ($n = 80$ cells from 6 head-fixed, anesthetized mice). **b**, Extinction of freezing behavior in freely running animals ($n = 6$ mice, obtained 1 d after conditioning). **c**, Comparison of reduction in cellular and behavioral response across CS ($\sum(\text{CS}_n - \text{CS}_{n+1}) / \sum \text{CS}_n$). $n = 6$ mice in each group (cellular versus behavioral response, $z = 2.3259$, $P = 0.02$; $*P < 0.05$, two-sided Wilcoxon rank-sum test). **d**, Experimental protocol for testing long-term persistence of astrocytic responsiveness. **e**, Top: Two-photon images of Fluo-8 AM-stained astrocytes from different control mice at days 1, 2 and 3 after conditioning. Responding cells are indicated by red circles, nonresponding ones by gray circles. The right-most panels present superimposed example traces of all tested astrocytes from the images in the corresponding row. The red number indicates responsive cells, the gray number nonresponsive ones. Bottom: Similar results obtained in conditioned animals. **f**, Same arrangement as in **e** showing results obtained at 13–15 d post-conditioning. **g**, Fraction of sound-responsive cells in three control (gray) and three conditioned groups (blue) at different days post-conditioning. The number of cells (and mice) are indicated in each bar graph (1–4 d: control versus post-conditioning, $z = -2.9530$, $P = 0.0031$; 5–8 d: control versus post-conditioning, $z = -2.9972$, $P = 0.0027$; 11–15 d: control versus post-conditioning, $z = -2.9912$, $P = 0.0028$; two-sided Wilcoxon rank-sum test, $**P < 0.01$). **h**, Fraction of sound-responsive cells in three conditioned groups before (blue, same as the conditioned groups in **g**) and after responsiveness extinction (black). The number of cells (and mice) are indicated in each bar graph (1–4 d: post-conditioning versus extinction, $z = 2.3749$, $P = 0.0176$; 5–8 d: post-conditioning versus extinction, $z = 2.2075$, $P = 0.0273$; 11–15 d: post-conditioning versus extinction, $z = 2.2014$, $P = 0.0277$; two-sided Wilcoxon signed-rank test, $*P < 0.05$). **i**, Amplitude of astrocytic Ca^{2+} transients in response to sound in three control (gray) and three conditioned groups (blue) at different days post-conditioning. The number of cells (and mice) are indicated in each bar graph (1–4 d: control versus post-conditioning, $z = -7.7169$, $P = 1.2 \times 10^{-14}$; 5–8 d: control versus post-conditioning, $z = -10.8959$, $P = 1.2 \times 10^{-27}$; 11–15 d: control versus post-conditioning, $z = -8.0813$, $P = 6.4 \times 10^{-16}$; two-sided Wilcoxon rank-sum test, $***P < 0.001$). **j**, Amplitude of astrocytic Ca^{2+} transients in three conditioned groups before (blue, same as the conditioned groups in **i**) and after responsiveness extinction (black). The number of cells (and mice) are indicated in each bar graph (1–4 d: post-conditioning versus extinction, $z = 4.5407$, $P = 5.6 \times 10^{-6}$; 5–8 d: post-conditioning versus extinction, $z = 4.7030$, $P = 2.6 \times 10^{-6}$; 11–15 d: post-conditioning versus extinction, $z = 5.5786$, $P = 2.4 \times 10^{-8}$; two-sided Wilcoxon signed-rank test, $***P < 0.001$). All data are shown as the mean \pm s.e.m.

for least 5–7 d post-conditioning in the experiments illustrated in Fig. 5d,f. After delivering ten CS to trained mice, a protocol that causes the extinction of freezing behavior (Supplementary Fig. 6)

(refs. ^{5,27}), both the fraction of sound-responding astrocytes and the amplitudes of sound-evoked Ca^{2+} transients returned to control levels (Fig. 6h,j). Together, our results demonstrate a remarkably tight



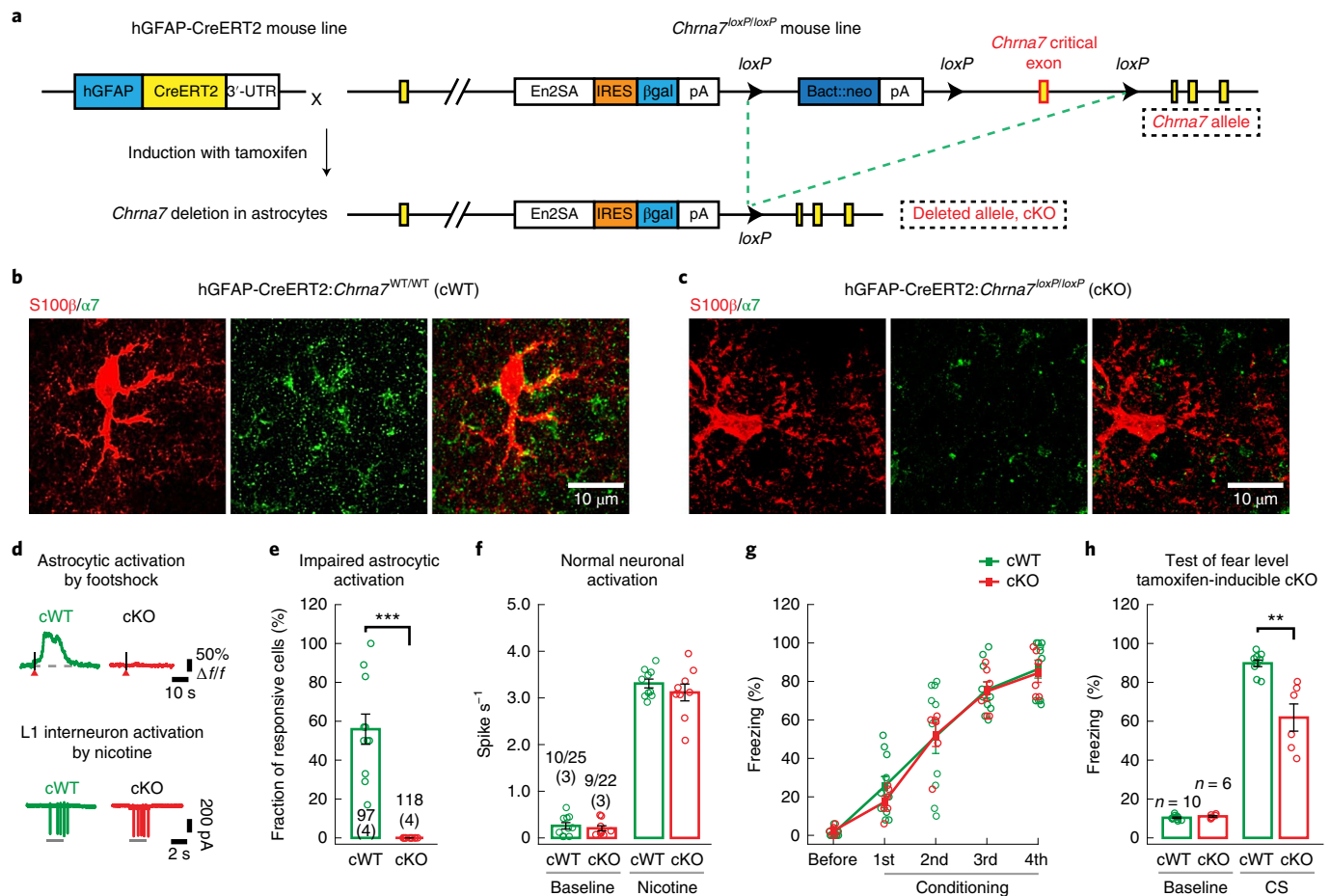


Fig. 7 | Impairment of fear memory persistence by tamoxifen-inducible deletion of the $\alpha 7$ subunit of nAChRs in astrocytes. **a**, Procedure for the generation of tamoxifen-inducible, astrocyte-specific $\alpha 7$ cKO mice. β gal, β -galactosidase; En2SA, En2 splice acceptor, IRES, internal ribosome entry site. **b,c**, Immunostaining of the $\alpha 7$ subunit of nAChRs and astrocytes (S100 β) in the auditory cortex of $\alpha 7$ cWT (**b**) and $\alpha 7$ cKO (**c**) mice. **d**, Top: Footshock-evoked responses in representative cortical astrocytes in $\alpha 7$ cWT (green) and $\alpha 7$ cKO (red) mice. Bottom: Nicotine-evoked spike responses in representative L1 interneurons in $\alpha 7$ cWT (green) and $\alpha 7$ cKO (red) mice. **e**, Summary of footshock-evoked responses in astrocytes. $n = 11$ fields of view (97 cells from 4 mice) in the cWT group; $n = 12$ fields of view (118 cells from 4 mice) in the cKO group (cWT versus cKO, $z = 4.3566$, $P = 1.3211 \times 10^{-5}$, two-sided Wilcoxon rank-sum test, *** $P < 0.001$). **f**, Summary of nicotine-evoked responses in L1 interneurons (spike frequency; $n = 10$ of 25 cells from 3 mice in the cWT group, $n = 9$ of 22 cells from 3 mice in the cKO group; baseline: cWT versus cKO, $z = 0.0409$, $P = 0.9674$; nicotine: cWT versus cKO, $z = 0.5307$, $P = 0.5956$, two-sided Wilcoxon rank-sum test). **g**, Freezing levels of cWT and cKO mice during fear conditioning ($n = 10$ mice in the cWT group, $n = 6$ mice in the cKO group). **h**, Summary of the freezing levels in both genotypes after fear conditioning ($n = 10$ mice in the cWT group, $n = 6$ mice in the cKO group; baseline: cWT versus cKO, $z = -1.2492$, $P = 0.2116$; CS: cWT versus cKO, $z = 3.1501$, $P = 0.0016$, two-sided Wilcoxon rank-sum test, ** $P < 0.01$). The number of tested cells (and mice) is indicated above each bar graph. All data are shown as the mean \pm s.e.m.

link between CS-dependent astrocytic Ca^{2+} responsiveness and freezing behavior during fear memory persistence. However, these results do not clarify whether nicotinic activation of astrocytes is directly involved in memory functions or represent just an associated ‘epiphenomenon’.

Deletion of astrocytic $\alpha 7$ -nAChRs impairs memory persistence.

To explore a possible causal role of astrocytic $\alpha 7$ -nAChRs in fear memory persistence, we generated tamoxifen-inducible, time-specific $\alpha 7$ -nAChR-deficient mice by crossing hGFAP-CreERT2 mice with mice whose sequence of the *Chrna7* gene is flanked by *loxP* sites (*Chrna7^{loxP/loxP}*) (Fig. 7a, Extended Data Fig. 9a and Supplementary Fig. 7; see also specificity and efficiency of Cre-mediated recombination in astrocytes in Supplementary Table 1). Like previous studies that used such hGFAP-CreERT2 mice to delete other types of receptors in astrocytes^{51,52}, immunostaining control experiments performed after tamoxifen injection (Fig. 7b,c; see also the overview images in Extended Data Fig. 9b,c) confirmed the effective

deletion of $\alpha 7$ -nAChRs in astrocytes in these conditional knockout (cKO) mice (hGFAP-CreERT2:*Chrna7^{loxP/loxP}*). In addition, we verified in control experiments involving immunoelectron microscopy that $\alpha 7$ -nAChRs were expressed in cortical astrocytes in conditional wild-type (cWT) mice but not in cKO mice, while they were present in the neurons of both genotypes (Supplementary Fig. 8). Astrocytes lacking $\alpha 7$ -nAChRs were unresponsive to footshock stimulation (Fig. 7d top and 7e). Another round of control experiments involved testing $\alpha 7$ -nAChRs in L1 interneurons of the auditory cortex, which are known to contribute decisively to fear learning^{26,27}. For this purpose, we used immunohistochemistry (Extended Data Fig. 9b,c left and 9d), in vivo electrophysiological (Fig. 7d, lower) and two-photon Ca^{2+} imaging recordings (Extended Data Fig. 9f–h). These experiments indicated a normal expression of $\alpha 7$ -nAChRs (Extended Data Fig. 9d) as well as the usual nicotine- and footshock-evoked responses in L1 interneurons of cKO mice (Fig. 7d, lower and 7f and Extended Data Fig. 9f–h). After establishing that cKO mice lack $\alpha 7$ -nAChRs specifically in astrocytes

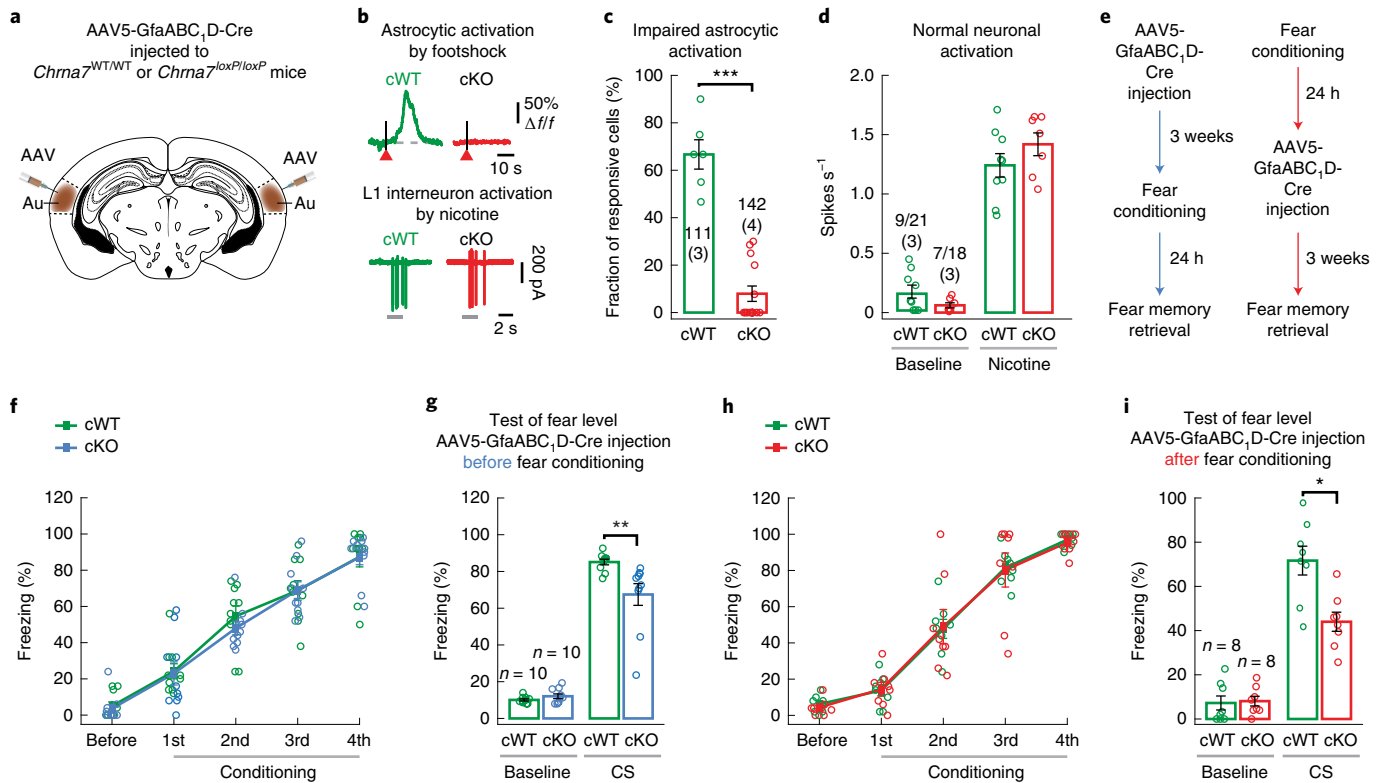


Fig. 8 | Impairment of fear memory persistence by auditory cortex-specific deletion of astrocytic $\alpha 7$ subunit of nAChRs. **a**, Schematic indicating the sites of bilateral viral injections in the auditory cortex. **b**, Footshock-evoked astrocytic responses (top) and nicotine-evoked neuronal responses (bottom) in cWT (AAV + *Chrna7*^{WT/WT}) and cKO (AAV + *Chrna7*^{loxP/loxP}). **c**, Summary of footshock-evoked responses in astrocytes. *n* = 6 fields of view (111 cells from 3 mice) in the cWT group; *n* = 14 fields of view (142 cells from 4 mice) in the cKO group (cWT versus cKO, $z = -3.5901$, $P = 3.3060 \times 10^{-4}$, two-sided Wilcoxon rank-sum test, ****P* < 0.001). **d**, Summary of nicotine-evoked responses in L1 interneurons (spike frequency; *n* = 9 of 21 cells from 3 mice in the cWT group, *n* = 7 of 18 cells from 3 mice in the cKO group; baseline: cWT versus cKO, $z = 1.2893$, $P = 0.1973$; nicotine: cWT versus cKO, $z = -1.1652$, $P = 0.2439$; two-sided Wilcoxon rank-sum test). **e**, Protocols of the fear behavior experiments in virus-induced, region-specific astrocytic $\alpha 7$ -nAChR cKO mice (AAV + *Chrna7*^{loxP/loxP}). AAV were injected before (left) and after (right) conditioning. **f**, Freezing levels of cWT and cKO mice during conditioning (AAV injection before conditioning, *n* = 10 mice in each group). **g**, Summary of freezing levels in both genotypes (AAV injection before conditioning, *n* = 10 mice in each group; baseline: cWT versus cKO, $z = -0.8776$, $P = 0.3802$; CS: cWT versus cKO, $z = 3.1773$, $P = 0.0015$; two-sided Wilcoxon rank-sum test, ***P* < 0.01). **h**, Freezing levels of cWT and cKO mice during conditioning (AAV injection after conditioning, *n* = 8 mice in each group). **i**, Summary of freezing levels in both genotypes (AAV injection after fear conditioning; *n* = 8 mice in each group; baseline: cWT versus cKO, $z = -0.7412$, $P = 0.4586$; CS: cWT versus cKO, $z = 2.5730$, $P = 0.0101$; two-sided Wilcoxon rank-sum test, **P* < 0.05). The number of tested cells (and mice) is indicated above each bar graph. All data are shown as the mean \pm s.e.m.

(Fig. 7d, upper and 7e and Extended Data Fig. 9b,c right and 9e), we performed behavioral tests. We found that cKO mice showed comparable learning abilities during fear conditioning (Fig. 7g) but had significantly reduced fear levels after fear learning compared to their cWT littermates (hGFAP-CreERT2:*Chrna7*^{WT/WT}) (Fig. 7h).

The cKO mice tested above may have had deletions of $\alpha 7$ -nAChRs not only in the auditory cortex but also in the astrocytes of other brain regions involved in some forms of fear learning and memory, such as the hippocampus or amygdala (Extended Data Figs. 7 and 8a–d). Therefore, to test for the specific contribution of auditory cortical astrocytes, we performed a region-specific deletion of $\alpha 7$ -nAChRs in astrocytes using a viral construct-mediated Cre/lox approach⁵¹. For this purpose, we bilaterally injected AAV5-GfaABC₁D-Cre⁵³ into the auditory cortices of adult *Chrna7*^{loxP/loxP} mice and their cWT littermates (Fig. 8a and Extended Data Fig. 10a). In the control experiments, we used immunostaining (Extended Data Fig. 10b–f) and in vivo functional analyses including electrophysiology and two-photon Ca²⁺ imaging (Fig. 8b–d and Extended Data Fig. 10g–i) to verify the deletion of $\alpha 7$ -nAChRs in astrocytes but the unchanged nicotinic responsiveness of L1 interneurons. Behaviorally, we performed two distinct

tests. In the first one, the injection of AAV5-GfaABC₁D-Cre into the auditory cortex was performed three weeks before fear conditioning (Fig. 8e left). In this situation, the deletion of $\alpha 7$ -nAChRs was completed at the time of pairing. While the fear learning process itself was not affected (Fig. 8f), the persistence of the learned fear levels was significantly impaired (Fig. 8g). In the second test, the injection of AAV5-GfaABC₁D-Cre into the auditory cortex was performed 24 h after fear conditioning but preceded memory retrieval by 3 weeks (Fig. 8e right). Thus, the pairing took place in conditions of an intact function of astrocytic $\alpha 7$ -nAChRs and fear learning was unaffected (Fig. 8h). However, fear levels were impaired three weeks after injection of the viral construct and associated deletion of astrocytic $\alpha 7$ -nAChRs (Fig. 8i). In sum, we conclude that astrocytic $\alpha 7$ -nAChRs in the auditory cortex are needed for memory persistence and retrieval.

Discussion

In the past decades, extensive efforts have been made to investigate the roles of astrocytes in learning and memory. Progress has emerged particularly with the development of advanced methods including genetically encoded molecular constructs for targeting

and manipulating astrocytes specifically *in vivo*⁵⁴. Thus, several recent studies have demonstrated the necessity of astrocytes in various memory functions. Most important are the insights obtained at the population level showing that interfering with normal astrocyte function can cause memory impairment, whereas activating them externally can lead to memory enhancement^{20,24}. In the present study, by monitoring astrocyte Ca²⁺ activity at the single-cell level over several days with *in vivo* two-photon Ca²⁺ imaging and at the level of small clusters with optic fiber-based recordings in freely moving mice, we discovered a new form of learning-induced astrocytic signaling. This occurs in a subset of astrocytes during fear learning, persists precisely along with the persistence of fear memory and vanishes directly with the extinction of the learned behavior. By using pharmacological, electrophysiological and molecular biological manipulations, we found that this astrocytic responsiveness required activation of $\alpha 7$ -nAChRs, which were activated by afferent cholinergic neuronal inputs. Genetic deletion of $\alpha 7$ -nAChRs specifically in astrocytes of the auditory cortex significantly impaired fear memory persistence. Therefore, the major added value of our study to the field is the identification of a new neuron–glia signaling mechanism in the cortex with a key contribution of these astrocytes to memory persistence. This role of astrocytes had not been anticipated in previous studies (for example, ref. 1).

Neuronal and glial contribution to memory persistence. Memory persistence has been largely attributed to neurons and considered to be due to a persistent change in the function of neurons and circuits based on experience, reflecting what had transpired at encoding and predicting what can be recovered during retrieval¹. In the case of auditory associative fear learning, afferent cholinergic inputs were shown to induce long-term modifications of synaptic plasticity in auditory cortex neurons^{26,27}. The long-term plastic modification of the function of cortical afferents to the amygdala is thought to contribute to the persistence of fear memory^{5,25}.

However, accumulating experimental evidence indicates that astrocytes can also actively modulate both synaptic transmission and plasticity^{7,8,18} and ultimately contribute to memory processing^{19–22}. Such astrocytic modulation is both circuit-⁵⁵ and stimulus-specific⁵⁶. Our present results indicate that a new form of glial signaling, consisting of learning-acquired Ca²⁺ responsiveness in a subset of cortical astrocytes, can serve as an essential cellular cosubstrate of fear memory⁵ since it is induced by the CS, persists for many days in tight association with the learned freezing response and vanishes with the extinction of the learned behavior. Importantly, the specific deletion of this *de novo*-induced astrocytic $\alpha 7$ -nAChR-mediated Ca²⁺ response impairs learned freezing responses.

Astrocytic Ca²⁺ responsiveness is $\alpha 7$ -nAChR-dependent. Cholinergic afferents from the basal forebrain to the cortex are classical modulators of cortical neuronal activity and synaptic plasticity and are required for fear learning and memory^{5,26,27}. Generally, the cholinergic effects are mediated through the activation of muscarinic⁵⁷ and/or nicotinic receptors^{26,27}. In addition to the well-established roles for neuronal activation and modulation, increasing evidence indicates that cholinergic activation of astrocytes through muscarinic receptors is involved in cortical and hippocampal plasticity^{13,18}. Additionally, an expression of $\alpha 7$ -nAChRs has been found in astrocytes of different brain regions including the hippocampus and cortex^{9,54,58}. *In vitro* recordings revealed nAChR-mediated Ca²⁺ transients in astrocytes that represent most likely $\alpha 7$ -nAChR-mediated signals generated by Ca²⁺-induced Ca²⁺ release from endoplasmic reticulum stores⁴¹.

Our present results demonstrate that Ca²⁺-induced Ca²⁺ release from endoplasmic reticulum stores is the signaling mechanism for sensory stimulation-evoked astrocytic Ca²⁺ responsiveness in the auditory cortex *in vivo*. Furthermore, we identified an essential

role of nicotinic receptors in cortical astrocytes for learning and memory. We demonstrated that both footshock- (unconditioned stimulus) and sound (CS)-induced Ca²⁺ transients in cortical astrocytes require $\alpha 7$ -nAChR activation. Astrocyte activation was purely afferent neuron-driven and thus different from the previously reported spontaneous astrocytic Ca²⁺ wave activity, which requires gap junction-dependent glia–glia communication⁴⁵. Moreover, unlike the astrocyte activation mechanism observed under a startle or vigilance condition^{43,46,47}, there was no norepinephrine-mediated contribution to the astrocytic responsiveness in the auditory cortex during footshock or sound stimulation. Also, the astrocytic responsiveness in the auditory cortex did not require metabotropic glutamate receptors whose activation is involved in the astrocytes of the somatosensory cortex during whisker stimulation¹². In summary, the cholinergic neuron–astrocyte circuit of the auditory cortex identified in our study is unique in many of its molecular and functional properties and well adapted for fear learning-dependent interactions with the previously reported nAChR-activated disinhibitory neuronal microcircuit in the auditory cortex^{26,27}. Possibly, while the neuronal microcircuit plays a prime role in the induction of the learning process and behavioral control, learning-induced changes in astrocytic responsiveness are key factors for fear memory maintenance and persistence.

Relevance and possible roles of astrocytes for memory. While glia have a major role in controlling metabolic processes in the brain, a rich previous body of evidence indicated that astrocytes are also involved in sensory integration and neural plasticity^{7,11,12,18,20,54}. The insights obtained in our study demonstrate that astrocytes are not only involved in the dynamic regulation of neuronal responses but can also play a key role in prolonged information storage in the brain, especially in conditions like those of fear learning, which involve the activation of large numbers of neurons in the cortex and elsewhere⁵. The contribution of astrocytes may consist of an adaptive control of synaptic processes in participating neurons^{7,8,18} as well as metabolic and hemodynamic regulation during the strong freezing behavior-associated increased neuronal activity¹¹. Since biological processes do not always reach their potential maxima, it is tempting to devise ways to enhance normal memory performance^{5,24}. In this study, we demonstrated that astrocytic activity integrates into stimulus convergence after memory formation and persistence and ultimately contributes to optimize memory performance. Considering that artificially manipulating astrocytes by a chemogenetic or optogenetic tool promotes memory allocation and improves memory performance²⁴, the requirement of $\alpha 7$ -nAChRs in astrocytes for memory persistence revealed in our study may represent an important molecular therapeutic target to fight against cognitive alterations or decline in many central nervous system diseases, such as amnesia, Alzheimer's disease and traumatic brain injury^{7,59}.

Online content

Any methods, additional references, Nature Research reporting summaries, source data, extended data, supplementary information, acknowledgements, peer review information; details of author contributions and competing interests; and statements of data and code availability are available at <https://doi.org/10.1038/s41593-021-00949-8>.

Received: 1 June 2020; Accepted: 27 September 2021;
Published online: 15 November 2021

References

1. Richards, B. A. & Frankland, P. W. The persistence and transience of memory. *Neuron* **94**, 1071–1084 (2017).
2. Albo, Z. & Gräff, J. The mysteries of remote memory. *Philos. Trans. R. Soc. Lond. B Biol. Sci.* **373**, 20170029 (2018).

3. Khan, Z. U., Martín-Montañez, E., Navarro-Lobato, I. & Muly, E. C. Memory deficits in aging and neurological diseases. *Prog. Mol. Biol. Transl. Sci.* **122**, 1–29 (2014).
4. Tonegawa, S., Morrissey, M. D. & Kitamura, T. The role of engram cells in the systems consolidation of memory. *Nat. Rev. Neurosci.* **19**, 485–498 (2018).
5. Maren, S. & Quirk, G. J. Neuronal signalling of fear memory. *Nat. Rev. Neurosci.* **5**, 844–852 (2004).
6. Bliss, T. V. & Collingridge, G. L. A synaptic model of memory: long-term potentiation in the hippocampus. *Nature* **361**, 31–39 (1993).
7. Santello, M., Toni, N. & Volterra, A. Astrocyte function from information processing to cognition and cognitive impairment. *Nat. Neurosci.* **22**, 154–166 (2019).
8. Haydon, P. G. & Nedergaard, M. How do astrocytes participate in neural plasticity? *Cold Spring Harb. Perspect. Biol.* **7**, a020438 (2014).
9. Zhang, K. et al. Sensory response of transplanted astrocytes in adult mammalian cortex in vivo. *Cereb. Cortex* **26**, 3690–3704 (2016).
10. Petzold, G. C., Albeanu, D. F., Sato, T. F. & Murthy, V. N. Coupling of neural activity to blood flow in olfactory glomeruli is mediated by astrocytic pathways. *Neuron* **58**, 897–910 (2008).
11. Schummers, J., Yu, H. & Sur, M. Tuned responses of astrocytes and their influence on hemodynamic signals in the visual cortex. *Science* **320**, 1638–1643 (2008).
12. Wang, X. et al. Astrocytic Ca²⁺ signaling evoked by sensory stimulation in vivo. *Nat. Neurosci.* **9**, 816–823 (2006).
13. Takata, N. et al. Astrocyte calcium signaling transforms cholinergic modulation to cortical plasticity in vivo. *J. Neurosci.* **31**, 18155–18165 (2011).
14. Panatier, A. et al. Astrocytes are endogenous regulators of basal transmission at central synapses. *Cell* **146**, 785–798 (2011).
15. Henneberger, C., Papouin, T., Oliet, S. H. & Rusakov, D. A. Long-term potentiation depends on release of D-serine from astrocytes. *Nature* **463**, 232–236 (2010).
16. Fellin, T. et al. Neuronal synchrony mediated by astrocytic glutamate through activation of extrasynaptic NMDA receptors. *Neuron* **43**, 729–743 (2004).
17. Kol, A. et al. Astrocytes contribute to remote memory formation by modulating hippocampal–cortical communication during learning. *Nat. Neurosci.* **23**, 1229–1239 (2020).
18. Navarrete, M. et al. Astrocytes mediate in vivo cholinergic-induced synaptic plasticity. *PLoS Biol.* **10**, e1001259 (2012).
19. Suzuki, A. et al. Astrocyte–neuron lactate transport is required for long-term memory formation. *Cell* **144**, 810–823 (2011).
20. Martín-Fernández, M. et al. Synapse-specific astrocyte gating of amygdala-related behavior. *Nat. Neurosci.* **20**, 1540–1548 (2017).
21. Orr, A. G. et al. Astrocytic adenosine receptor A2A and Gs-coupled signaling regulate memory. *Nat. Neurosci.* **18**, 423–434 (2015).
22. Robin, L. M. et al. Astroglial CB₁ receptors determine synaptic D-serine availability to enable recognition memory. *Neuron* **98**, 935–944.e5 (2018).
23. Han, X. et al. Forebrain engraftment by human glial progenitor cells enhances synaptic plasticity and learning in adult mice. *Cell Stem Cell* **12**, 342–353 (2013).
24. Adamsky, A. et al. Astrocytic activation generates de novo neuronal potentiation and memory enhancement. *Cell* **174**, 59–71.e14 (2018).
25. Dalmay, T. et al. A critical role for neocortical processing of threat memory. *Neuron* **104**, 1180–1194.e7 (2019).
26. Guo, W., Robert, B. & Polley, D. B. The cholinergic basal forebrain links auditory stimuli with delayed reinforcement to support learning. *Neuron* **103**, 1164–1177.e6 (2019).
27. Letzkus, J. J. et al. A disinhibitory microcircuit for associative fear learning in the auditory cortex. *Nature* **480**, 331–335 (2011).
28. Hirase, H., Qian, L., Barthó, P. & Buzsáki, G. Calcium dynamics of cortical astrocytic networks in vivo. *PLoS Biol.* **2**, E96 (2004).
29. Yao, J. et al. A corticopontine circuit for initiation of urination. *Nat. Neurosci.* **21**, 1541–1550 (2018).
30. Qin, H. et al. A visual-cue-dependent memory circuit for place navigation. *Neuron* **99**, 47–55.e4 (2018).
31. Nimmerjahn, A., Kirchhoff, F., Kerr, J. N. & Helmchen, F. Sulforhodamine 101 as a specific marker of astroglia in the neocortex in vivo. *Nat. Methods* **1**, 31–37 (2004).
32. Thrane, A. S. et al. General anesthesia selectively disrupts astrocyte calcium signaling in the awake mouse cortex. *Proc. Natl Acad. Sci. USA* **109**, 18974–18979 (2012).
33. Chen, T.-W. et al. Ultrasensitive fluorescent proteins for imaging neuronal activity. *Nature* **499**, 295–300 (2013).
34. Stobart, J. L. et al. Cortical circuit activity evokes rapid astrocyte calcium signals on a similar timescale to neurons. *Neuron* **98**, 726–735.e4 (2018).
35. Stobart, J. L. et al. Long-term in vivo calcium imaging of astrocytes reveals distinct cellular compartment responses to sensory stimulation. *Cereb. Cortex* **28**, 184–198 (2018).
36. Chen, X., Leischner, U., Rochefort, N. L., Nelken, I. & Konnerth, A. Functional mapping of single spines in cortical neurons in vivo. *Nature* **475**, 501–505 (2011).
37. Rothschild, G., Nelken, I. & Mizrahi, A. Functional organization and population dynamics in the mouse primary auditory cortex. *Nat. Neurosci.* **13**, 353–360 (2010).
38. Li, J. et al. Primary auditory cortex is required for anticipatory motor response. *Cereb. Cortex* **27**, 3254–3271 (2017).
39. Tischbirek, C. H. et al. In vivo functional mapping of a cortical column at single-neuron resolution. *Cell Rep.* **27**, 1319–1326.e5 (2019).
40. Wang, M. et al. Single-neuron representation of learned complex sounds in the auditory cortex. *Nat. Commun.* **11**, 4361 (2020).
41. Sharma, G. & Vijayaraghavan, S. Nicotinic cholinergic signaling in hippocampal astrocytes involves calcium-induced calcium release from intracellular stores. *Proc. Natl Acad. Sci. USA* **98**, 4148–4153 (2001).
42. Srinivasan, R. et al. New transgenic mouse lines for selectively targeting astrocytes and studying calcium signals in astrocyte processes in situ and in vivo. *Neuron* **92**, 1181–1195 (2016).
43. Bekar, L. K., He, W. & Nedergaard, M. Locus coeruleus α -adrenergic-mediated activation of cortical astrocytes in vivo. *Cereb. Cortex* **18**, 2789–2795 (2008).
44. Ding, F. et al. α 1-Adrenergic receptors mediate coordinated Ca²⁺ signaling of cortical astrocytes in awake, behaving mice. *Cell Calcium* **54**, 387–394 (2013).
45. Kuga, N., Sasaki, T., Takahara, Y., Matsuki, N. & Ikegaya, Y. Large-scale calcium waves traveling through astrocytic networks in vivo. *J. Neurosci.* **31**, 2607–2614 (2011).
46. Paukert, M. et al. Norepinephrine controls astroglial responsiveness to local circuit activity. *Neuron* **82**, 1263–1270 (2014).
47. Oe, Y. et al. Distinct temporal integration of noradrenaline signaling by astrocytic second messengers during vigilance. *Nat. Commun.* **11**, 471 (2020).
48. Huerta, P. T., Sun, L. D., Wilson, M. A. & Tonegawa, S. Formation of temporal memory requires NMDA receptors within CA1 pyramidal neurons. *Neuron* **25**, 473–480 (2000).
49. Grienberger, C. et al. Sound-evoked network calcium transients in mouse auditory cortex in vivo. *J. Physiol.* **590**, 899–918 (2012).
50. Ghosh, S. & Chattarji, S. Neuronal encoding of the switch from specific to generalized fear. *Nat. Neurosci.* **18**, 112–120 (2015).
51. García-Cáceres, C. et al. Astrocytic insulin signaling couples brain glucose uptake with nutrient availability. *Cell* **166**, 867–880 (2016).
52. Kim, J. G. et al. Leptin signaling in astrocytes regulates hypothalamic neuronal circuits and feeding. *Nat. Neurosci.* **17**, 908–910 (2014).
53. Nagai, J. et al. Hyperactivity with disrupted attention by activation of an astrocyte synaptogenic cue. *Cell* **177**, 1280–1292.e20 (2019).
54. Zhang, K. & Chen, X. Sensory response in host and engrafted astrocytes of adult brain in vivo. *Glia* **65**, 1867–1884 (2017).
55. Martín, R., Bajo-Grañeras, R., Moratalla, R., Perea, G. & Araque, A. Circuit-specific signaling in astrocyte–neuron networks in basal ganglia pathways. *Science* **349**, 730–734 (2015).
56. Mariotti, L. et al. Interneuron-specific signaling evokes distinctive somatostatin-mediated responses in adult cortical astrocytes. *Nat. Commun.* **9**, 82 (2018).
57. Froemke, R. C. et al. Long-term modification of cortical synapses improves sensory reception. *Nat. Neurosci.* **16**, 79–88 (2013).
58. Duffy, A. M. et al. Acetylcholine α 7 nicotinic and dopamine D₂ receptors are targeted to many of the same postsynaptic dendrites and astrocytes in the rodent prefrontal cortex. *Synapse* **65**, 1350–1367 (2011).
59. Blanco-Suárez, E., Caldwell, A. L. M. & Allen, N. J. Role of astrocyte–synapse interactions in CNS disorders. *J. Physiol.* **595**, 1903–1916 (2017).

Publisher's note Springer Nature remains neutral with regard to jurisdictional claims in published maps and institutional affiliations.

© The Author(s), under exclusive licence to Springer Nature America, Inc. 2021

Methods

Mice. C57BL/6 mice were obtained from the Laboratory Animal Center at the Third Military Medical University. C57BL/6N-*Chrna7^{tm1a(EUCOMM)Hmg}*/H mice were obtained from the European Mouse Mutant Archive (EM:07778). B6.Cg-Tg(GFAP-Cre/ERT2)505Fmv/J (strain no. 012849) and B6.Cg-Gi(ROSA)26Sor^{tm1a(CAG-tdTomato)Hze/J} (strain no. 007914) mice were obtained from The Jackson Laboratory. Male, 8–12-week-old mice were used in this study. Mice were housed on a 12-h light–dark cycle, at 22–25°C and in 50–60% relative humidity with ad libitum access to food and water. All animal experiments were carried out in accordance with the regulations of the German Animal Welfare Act; protocols were approved by the government of Bavaria, Germany and by the Institutional Animal Care and Use Committee of the Third Military Medical University.

In vivo two-photon Ca²⁺ imaging of cortical astrocytes. For the two-photon Ca²⁺ imaging experiments, surgery and recordings were performed as described previously⁹. Briefly, mice were placed onto warming plates (37–38°C) and anesthetized by inhalation of 1–1.5% isoflurane (Curamed or RWD Life Science) in pure O₂. The skin and soft tissues were removed under a dissecting microscope after local application of xylocaine. A custom-made recording chamber was then glued to the skull of each animal. A craniotomy (approximately 1 × 1 mm) centered on the left auditory cortex (bregma –2.5 mm, 4.5–4.9 mm lateral to midline; the coordinates leading to the dye staining area often covered the primary auditory cortex, ventral secondary auditory cortex and part of the adjacent temporal association cortex²⁵) or the left primary somatosensory cortex (bregma –0.56 mm, 1.65 mm lateral to midline) was made using a high-speed drill with a small tip steel burr (0.45 mm in diameter). The craniotomy was filled with 1–1.5% low melting point agarose to minimize brain pulsation. After surgery, each mouse was transferred into the recording apparatus and the anesthesia level was decreased to 0.5% isoflurane in pure O₂ (breathing rate was around 120 breaths per minute). The recording chamber was perfused with warm normal artificial cerebrospinal fluid (ACSF) containing 125 mM of NaCl, 4.5 mM of KCl, 26 mM of NaHCO₃, 1.25 mM of NaH₂PO₄, 2 mM of CaCl₂, 1 mM of MgCl₂ and 20 mM of glucose, pH 7.4, when bubbled with 95% O₂ and 5% CO₂. The temperature of each mouse was maintained in the range of 36.5–37.5°C throughout the recording.

The Ca²⁺ indicators Fluo-8 AM (catalog no. 21081; AAT Bioquest), Rhod-2 AM (catalog no. R1244, Invitrogen; Extended Data Fig. 5a) or Cal-520 AM (catalog no. 21131; AAT Bioquest; Extended Data Figs. 9f and 10g) were used for the bulk-loading procedure, which was adapted and further developed based on previous reports²⁸. Fluo-8 AM, Rhod-2 AM or Cal-520 AM were dissolved in dimethyl sulfoxide with 20% pluronic F-127 and diluted with the normal ACSF solution to a final concentration of approximately 0.5 mM. The final solutions of Fluo-8 AM or Cal-520 AM were applied locally into the target region by pressure (approximately 400 mbar, 2–4 min) using a glass pipette. One hour was required for dye loading of astrocytes or neurons. For Rhod-2 AM, the final solution was loaded on the exposed area for 10 min, followed by a 30-min wash with ACSF. In some experiments, the exposed area was also loaded with sulforhodamine 101 by surface application after Ca²⁺ imaging to confirm the specificity of labeling³¹.

Two-photon Ca²⁺ imaging of astrocytes was performed with a custom-built two-photon microscope system similar to that reported previously by Zhang et al.⁹. In this system, the scanner was mounted on an upright microscope (BX61WI; Olympus) equipped with a water immersion objective (40×/0.80 numerical aperture; Nikon). Full-frame images were acquired at 40 frames s⁻¹ by custom-written software based on LabVIEW (National Instruments). The wavelength of the excitation laser was set at 920 nm for the imaging of Fluo-8 AM-labeled astrocytes and Cal-520 AM-labeled neurons or at 825 nm for Rhod-2 AM-labeled astrocytes. The average power delivered to the brain was adjusted to 20–50 mW depending on image depth.

In vivo electrophysiology. Local field potential recordings and cell-attached patch clamp recordings were obtained with an EPC10 amplifier (HEKA Elektronik) under two-photon imaging guidance. The patch pipette solution contained normal ACSF solution with 50 μM of AF594 (catalog no. A10438; Invitrogen) for local field potential or cell-attached recordings. We used the shadow patching approach for cell-attached patch clamp recording of neurons.

Pharmacological manipulation under two-photon imaging. For local drug application, a glass pipette filled with a mixture of the pharmacological agent and AF594 (50 μM) was placed in the field of imaging under two-photon imaging guidance⁹. The resistance of the pipette (4–6 MΩ) was continuously monitored before, during and after drug application. The drug and AF594 were coreleased by gentle pressure application (Picospritzer III; General Valve). The drug was injected at the following concentration: 50 μM of CPA, 10 μM of thapsigargin, 50 μM of ryanodine, 100 μM of MLA, 100 μM of VU0255035, 100 μM of MPEP, 200 μM of LY367385, 100 μM of APV, 100 μM of CNQX, 100 μM of nicotine, 0.5 μM of TTX, 50 μM of phentolamine, 200 μM of prazosin and 100 μM of carboxonolone.

Fear conditioning and behavior. We used an associative fear conditioning paradigm where a CS (an auditory cue) was paired with the presentation of an unconditioned aversive stimulus (a footshock). Conditioned stimuli were 9.9-s

trains of pure tone (8 kHz, 70 dB sound pressure level), consisting of 33 square pulses of 50 ms duration with and interpulse interval of 250 ms. The unconditioned stimulus was footshock for 1 s (0.6–1 mA). The onset of footshock coincided with the end of the last pulse of sound. The interval between two pairings was 3 min. For the experiments where fear conditioning was performed under a two-photon microscope (for example, Fig. 3a–f), we applied footshocks to the hind paws and presented sound from an electrostatic speaker (ES1; Tucker-Davis Technologies) placed approximately 5 cm away from the contralateral ear. Fear conditioning, inducing freezing behavior when tested during wakefulness (for example, Fig. 6), was effectively achieved by presentations of 10–15 pairings under anesthesia (0.5–0.8% isoflurane). For the experiments where fear conditioning was performed during wakefulness, we used a custom-made cage consisting of a 30 × 20 × 20-cm plastic box equipped with stainless steel shocking floor grids connected to a feedback current-regulated shocker (conditioning box). A charge-coupled device (CCD) camera (frame rate of 30 Hz) with infrared illumination and an electrostatic speaker were placed on the top and side wall of the box, respectively. Before the day of fear conditioning, mice were handled by the experimenter gently for 5 min per day for 3 d. In addition, on the conditioning day, mice were habituated for 5–10 min on the shocking grids in the cage before pairing. Three to five pairings were delivered with an interval of 3 min to induce fear conditioning. Mice were returned to their home cages 5 min after pairing. Over 1–15 d after conditioning, mice were subjected to either fear retrieval for the fiber recordings (for example, Fig. 5) or behavioral tests (for example, Supplementary Fig. 6) in a different context with nonshocking grids or for two-photon imaging under the microscope. All equipment was completely cleaned with ethanol, followed by water rinsing, between sessions.

To test whether the response was specific to the trained CS⁺ tone, we used CS⁺ (9.9-s trains of pure tone, 50-ms duration for each pulse of sound, 33 pulses; 8 kHz, 70 dB sound pressure level) and CS⁻ (9.9-s trains of pure tone, 2 kHz, 70 dB sound pressure level) tones in the experiments. The CS⁺ tone was paired with the presentation of an unconditioned aversive stimulus (a footshock) during fear conditioning. Three to five pairings were delivered with an interval of 3 min for fear conditioning. The CS⁻ tone was never paired with a footshock. One or 7 d after fear conditioning, mice were subjected to fear retrieval in the presence of CS⁺ or CS⁻ tones for both behavioral tests and fiber recordings in a different context with nonshocking grids (Fig. 5). In the control experiments, we alternated the identity of CS⁺ and CS⁻ tones by using 2 kHz as CS⁺ and 8 kHz as CS⁻ (Supplementary Fig. 5). The freezing behavior tests were recorded by an infrared CCD camera and analyzed offline. Mice were considered to be freezing if no movement was detected for a duration of 2 s. The freezing level (Figs. 4–8, Extended Data Figs. 7 and 8 and Supplementary Figs. 5 and 6) was expressed as a percentage of time spent freezing²⁷. To ensure that our automatic system scored freezing rather than just immobility, we compared it previously with a classical time sampling procedure during which an experimenter blind to the experimental conditions determined if the mice were freezing or not every 2 s (defined as the complete absence of movement except for respiratory movements). The values obtained by the classical time sampling procedure were 95% identical with the automatic detection system, which was therefore used throughout the experimental sessions.

Virus injection for the expression of GCaMP6s or GCaMP6f. C57BL/6 mice were anesthetized with isoflurane (1–1.5% for surgery in pure O₂) and placed in a stereotaxic frame, as described previously^{29,30}. A small vertical incision was made in the skin. The skull directly above the injection site was thinned to allow penetration by a glass micropipette containing pAAV. Both AAV constructs (pAAV9-sGFAP-GCaMP6s^{34,35}, AAV5-GfaABC,D-cytoGCaMP6f-SV40 (catalog no. AV-5-52925; Penn Vector Core Transfer)^{24,53}) were injected with a volume of 800 nl per site without dilution. The AAV vectors were driven by the astrocyte-specific sGFAP or GfaABC,D promoter (a shorter 681-bp GFAP promoter)⁵³. We injected the pAAV with a micropipette using a micromanipulator (H. Saur) fixed on a custom-made platform. In steps of 100-μm depth we applied in total 150–300 nl of the viral construct at a rate of 0.1 μl min⁻¹. After the injection, the pipette was held in place for 15 min before being slowly retracted from the brain. The scalp incision was closed with tissue adhesive (Vetbond; 3M Animal Care Products); postinjection analgesics were given to aid recovery. Two-photon imaging experiments or optical fiber-based recordings were performed approximately 20 d after viral injection. The GCaMP6 injection sites were chosen according to the aims of the experiments: the auditory cortex (anterior–posterior (AP) –3.10 mm, mediolateral (ML) ± 3.80 mm, dorsoventral (DV) –1.30 mm with a 20-degree slope below the cortical surface for two-photon imaging; AP –2.54 mm, ML ± 4.6 mm, DV 0 to –0.9 mm for the optic fiber recordings³²), the primary somatosensory cortex (AP –0.56 mm, ML ± 1.65 mm, DV –0.3 mm), the CA1 of the hippocampus (AP –2.06 mm, ML ± 1.60 mm, DV –1.1 mm), the dorsal hippocampus (AP –1.7 mm, ML ± 1.8 mm, DV –2.0 mm) and the BLA in the amygdala (AP –1.6 mm, ML ± 3.1 mm, DV –5.0 mm).

Optic fiber-based recordings in freely moving mice. For fiber implantation surgery, mice labeled with GCaMP6f were anesthetized with isoflurane and placed in a stereotaxic head frame. An optical fiber (diameter of 200 μm, numerical aperture 0.48; catalog no. MFP_200/230/900-0.48; Doric) was inserted into

the location where the pAAV was injected, then fixed to the skull with dental cement (Tetric EvoFlow; Ivoclar Vivadent Corporate). For the different aims of the experiments, optic fiber ends were inserted at the following coordinates: the auditory cortex (AP -2.54 mm, ML ± 4.6 mm, DV -0.2 to -0.4 mm)²⁵; the primary somatosensory cortex (AP -0.56 mm, ML ± 1.65 mm, DV -0.3 mm); the CA1 of the hippocampus (AP -2.06 mm, ML ± 1.60 mm, DV -1.1 mm); the dorsal hippocampus (AP -1.7 mm, ML ± 1.8 mm, DV -2.0 mm); and the BLA in the amygdala (AP -1.6 mm, ML ± 3.1 mm, DV -5.0 mm). Optical fiber-based Ca²⁺ recordings were achieved using a modular fiber-optic device, as described previously^{29,30}. The fluorescence signals were sampled at 2000 Hz with custom-written software based on LabVIEW. Animal behavior was simultaneously monitored with a camera (frame rate of 30 Hz) under infrared illumination. The optical fiber recordings started after the 3-d handling of animals (5-min handling per day) by the experimenter. On each recording day, mice were habituated for 5–10 min on the shocking cage before the experiments. After the end of the fiber recording experiments, mice were killed for histological verification. After perfusion with 4% paraformaldehyde (PFA) and dehydration with 15% sucrose for 1 night, brains were cut into 50- μ m slices for imaging with a confocal microscope (LSM 700; ZEISS) or a stereoscope (Olympus) (Supplementary Fig. 4).

AAV-mediated astrocytic nAChR deletion in the auditory cortex. *LoxP-Chrna7* transgenic mice, also known as *Chrna7^{loxP/loxP}* (C57BL/6N-*Chrna7^{mla}*(EUCOMM)^{Hmgg/H}), obtained from EMMMA (EM:07778), were injected with AAV5-GfaABC,D-PI-Cre-SV40 (a gift from B. Khakh; Addgene plasmid no. 105603; Research Resource Identifier: Addgene_105603) (ref. ³³) into the auditory cortex (AP -2.54 mm, ML ± 4.6 mm, DV -0.8 mm)²⁵. The AAV vectors were driven by the astrocyte-specific GfaABC,D promoter³³ to excise *loxP* sites by Cre recombination. We performed the subsequent behavioral experiments with these mice three weeks after viral injection.

Transgenic mice and tamoxifen induction. hGFAP-CreERT2:*Chrna7^{loxP/loxP}* ($\alpha 7$ -cKO) transgenic mice were generated by crossing hGFAP-CreERT2 transgenic mice^{31,32} with *loxP-Chrna7* transgenic mice (*Chrna7^{loxP/loxP}*). hGFAP-CreERT2:*Chrna7^{WT/WT}* transgenic mice ($\alpha 7$ -cWT) from the same littermates were used as the control group. hGFAP-CreERT2:tdTomato^{loxP/loxP} transgenic mice were generated by crossing hGFAP-CreERT2 transgenic mice with *loxP*-tdTomato transgenic mice. To excise the *loxP* sites by Cre recombination, 5-week-old male mice were administered tamoxifen once daily (100 mg kg⁻¹ intraperitoneally) for 5–8 d. Tamoxifen (Sigma-Aldrich) was dissolved in sunflower oil at a final concentration of 10 mg ml⁻¹ at 37 °C and then filter-sterilized and stored for up to 7 d at 4 °C in the dark. All control groups were tamoxifen-injected littermate control mice ($\alpha 7$ -cWT). We performed experiments with these mice three weeks after the last injection of tamoxifen.

Histology and confocal imaging. For immunohistochemistry, mice were killed by delivery of an isoflurane overdose or by intraperitoneal injection of sodium pentobarbital and transcardially perfused with 4% PFA. Brains were removed, fixed overnight in 4% PFA and cryoprotected in 30% sucrose. Coronal brain sections (30 μ m) were prepared and stained as described previously^{29,30}. Briefly, sections were blocked at room temperature for 30 min in 10% normal goat serum, 1% bovine serum albumin, 0.3% Triton X-100 in PBS and incubated with primary antibodies overnight at 4 °C (goat anti-GFAP, 1:500 dilution, catalog no. ab53554, Abcam; rabbit anti-NeuN, 1:500 dilution, catalog no. ab177487, Abcam; mouse anti- $\alpha 7$ -nAChR, 1:300 dilution, catalog no. M220, Sigma-Aldrich; rabbit anti-S100 β , 1:500 dilution, catalog no. 287003, Synaptic Systems; chicken anti-GFP, 1:500 dilution, catalog no. ab13970, Abcam). Sections were rinsed in PBS, followed by incubation with secondary antibodies directed against the immunoglobulins of the appropriate species coupled to AF594 and AF488 (1:500 dilution, Invitrogen; 1:200 dilution, Jackson ImmunoResearch). Images were acquired with a Leica TCS SP5 confocal microscope (Leica Microsystems) equipped with standard filter sets and oil immersion objectives (60 \times /1.42 and 20 \times /0.85).

Immunoelectron microscopy. hGFAP-CreERT2:*Chrna7^{WT/WT}* ($\alpha 7$ -cWT) and hGFAP-CreERT2:*Chrna7^{loxP/loxP}* ($\alpha 7$ -cKO) mice were anesthetized with 1% sodium pentobarbital intraperitoneally and perfused transcardially with 20 ml of saline, followed by a 100-ml ice-cold mixture of 4% PFA and 0.75% glutaraldehyde in 0.1 M phosphate buffer (PB) for 40 min. Brains were removed and post-fixed by immersion in the same fixative without glutaraldehyde for 4 h at 4 °C. Serial coronal sections of 50- μ m thickness were prepared with a vibratome (MicroSlicer DTK-1000; Dosaka EMCo); then, approximately 18–20 sections, including the auditory cortex region, were collected from each brain. $\alpha 7$ -nAChR was detected by immunogold-silver staining. S100 β was detected by 3,3'-diaminobenzidine staining. Briefly, sections were treated with blocking buffer, 0.05 M Tris-buffered saline (TBS), pH 7.4, containing 20% (v/v) normal donkey serum for 40 min and then incubated overnight with mouse anti- $\alpha 7$ -nAChR antibodies (1:300 dilution) and rabbit anti-S100 β antibody (1:500 dilution) diluted with 0.05 M TBS containing 2% (v/v) normal donkey serum. The secondary antibody was an anti-mouse Nanogold-IgG goat anti-mouse IgG antibody (catalog no. 2001, 1:100 dilution; Nanoprobes) and biotin-SP conjugate donkey anti-rabbit IgG antibody

(1:200 dilution, catalog no. AP182B; Sigma-Aldrich) for 4 h. Silver enhancement was performed in the dark with a high-quality silver enhancement kit (catalog no. 2012; Nanoprobes) for visualization of $\alpha 7$ -nAChR immunoreactivity. Before and after the silver enhancement step, sections were rinsed several times with deionized water. Then, sections were incubated in the avidin-biotin peroxidase complex (ABC standard kit) for 45 min (1:100 dilution in 0.01 M PBS for each solution). To visualize the reaction product, sections were incubated in diaminobenzidine (4-mg tablet dissolved in 20 ml of 0.5 M Tris-HCl and 2 μ l of 30% hydrogen peroxide). Immunolabeled sections were then fixed with 1% osmium tetroxide in 0.1 M PB for 40 min, dehydrated in graded ethanol series and then in propylene oxide and finally flat-embedded in EPON 812 between sheets of plastic. After polymerization, acrylic sheets were then peeled from the polymerized resin and flat-embedded sections were examined under a light microscope. Three to four sections containing $\alpha 7$ -nAChR and S100 β immunoreactivity were selected from each brain, trimmed under a stereomicroscope and glued onto blank resin stubs. Serial ultrathin sections were cut with an Ultramicrotome (UC7; Leica Microsystems) using a diamond knife (Diatome) and mounted on formvar-coated mesh grids (6–8 sections per grid). They were then counterstained with uranyl and lead citrate and observed under a JEM-1400 electron microscope (JEOL) equipped with a CCD camera (Olympus Veleta) and its application software (ITEM 5.2; EMSIS).

Data analysis and quantification. Electrophysiological data were sampled at 50 kHz and filtered at 10 kHz using the PatchMaster software (version 2x65; HEKA Elektronik). Data analyses were done using LabVIEW 2014 (National Instruments), MATLAB 2014a (MathWorks) or Igor Pro 5.0 (version 6.0.3.1; WaveMetrics) in conjunction with custom-written macros⁹. Astrocytic Ca²⁺ transients were expressed as relative fluorescence changes ($\Delta f/f$), corresponding to the mean fluorescence from all pixels within specified regions of interest (ROIs), as described previously⁹. To extract the fluorescence signals, we visually identified astrocytes and drew ROIs based on fluorescence intensity. The Ca²⁺ signal for each ROI was expressed as $\Delta f/f = (f - f_0)/f_0$, where the baseline fluorescence f_0 was estimated as the 25th percentile of the entire fluorescence recording. Astrocytes were defined as 'responders' (Fig. 1 and Extended Data Fig. 2) when the maxima of the averaged Ca²⁺ signals from 3 consecutive trials 0–9 s after the stimuli were above 3 \times s.d. of the baseline. Therefore, 'nonresponders' should include weak responses that were smaller than 3 \times s.d. of the baseline traces. Fiber-based Ca²⁺ recording data were analyzed according to a previously established procedure^{29,30}.

Statistics and reproducibility. For all experiments, samples were randomized where appropriate for data collection and analysis. Experiments were repeated multiple times on independent occasions as indicated in the Methods and/or figure legends. All attempts at replication were successful. For optical fiber-based Ca²⁺ recordings, any mice whose virus injection sites or fiber tip sites were missed were excluded from the data analysis. Investigators were blinded to the groups for data collection and analysis. No statistical methods were used to predetermine sample sizes but our sample sizes were similar to those reported in our previous publications using similar methodology^{29,30}. Data were expressed as the mean \pm s.e.m. We used nonparametric statistical tests to compare central tendencies between two data groups. For paired and unpaired cases, we used a two-sided Wilcoxon signed-rank test and two-sided Wilcoxon rank-sum test, respectively. Group comparisons were made using two-way analysis of variance (ANOVA) followed by Bonferroni post hoc tests to control for multiple comparisons. Spearman correlation was used to calculate the correlation between amplitudes of astrocytic Ca²⁺ transients evoked by sound and footshock stimulation or between amplitudes of astrocytic Ca²⁺ transients and freezing levels in response to sound after fear conditioning. $P < 0.05$ was considered statistically significant. For the representative micrographs in Fig. 7b,c, Extended Data Figs. 2e, 9b,c and 10b,c and Supplementary Fig. 1b, experiments were repeated independently in 4–5 mice.

Reporting Summary. Further information on research design is available in the Nature Research Reporting Summary linked to this article.

Data availability

Any data generated and/or analyzed during the current study are available from the corresponding author upon reasonable request. No datasets that require mandatory deposition into a public database were generated during the current study. Source data underlying Figs. 1–8 and Extended Data Figs. 2–4 and 6–10 and Supplementary Figs. 5 and 6 are available as source data files. Source data are provided with this paper.

Code availability

No unique code was generated in this study. Source data are provided with this paper.

Acknowledgements

We thank J. Lou for technical assistance. B.W. is a member of the Clinical Research Priority Program Molecular Imaging Network Zurich. This work was supported by the National Key R&D Program of China (no. 2018YFA0109600), the National Natural Science Foundation of China (no. 81771175) and the program of the China Scholarship

Council (no. 201803170004) to K.Z., the National Natural Science Foundation of China (nos. 31925018, 31861143038, 31921003, 81671106) and Chongqing Basic Research grants (nos. cstc2019jcyjX0001 and cstc2019jcyj-cxttX0005) to X.C., the Deutsche Forschungsgemeinschaft (SFB870) and a European Research Council Advanced Grant to A.K. X.C. is a member of the CAS Center for Excellence in Brain Science and Intelligence Technology. A.K. is a Hertie Senior Professor of Neuroscience.

Author contributions

A.K. and X.C. designed the study. K.Z., R.F., W.H., J.L., C.Y., H.Q., M.W., R.D., R.L., T.J., Y.W., J.Z., Z.Y., Y.Z., J.S., B.W., H.A., A.K. and X.C. performed the main experiments. Y.L. and T.C. performed the immunoelectron microscopy experiments. S.Q. verified the astrocyte-specific Cre recombination of hGFAP-CreERT2:tdTomato^{loxP/loxP} mice. K.Z., R.F., J.L., C.Y., X.L., H.A. W.J. and X.C. performed the data analysis. A.K., X.C. and K.Z. wrote the manuscript with input from all coauthors.

Competing interests

The authors declare no competing interests.

Additional information

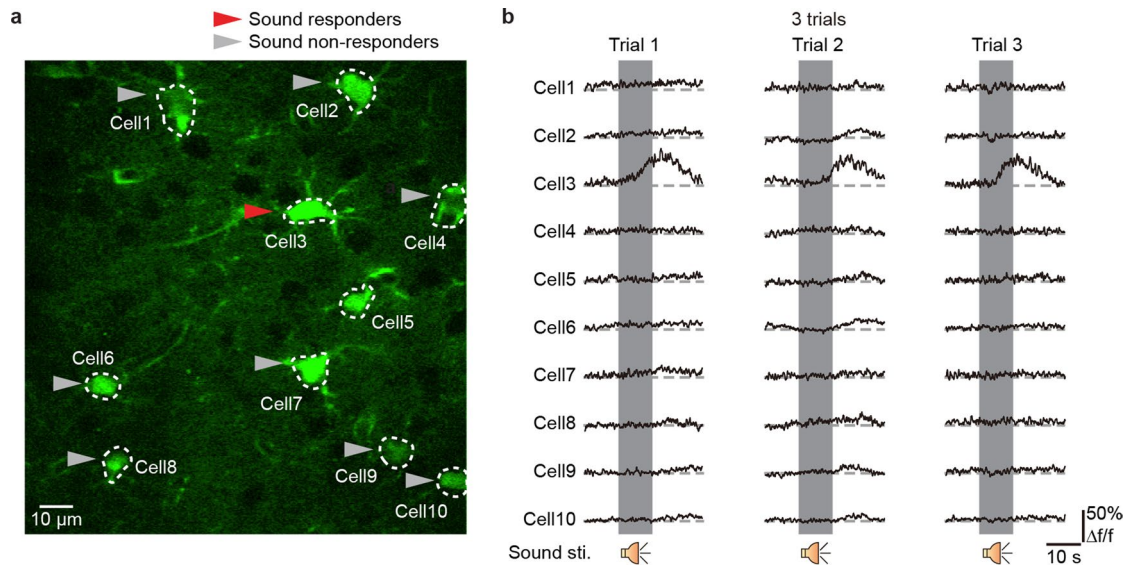
Extended data is available for this paper at <https://doi.org/10.1038/s41593-021-00949-8>.

Supplementary information The online version contains supplementary material available at <https://doi.org/10.1038/s41593-021-00949-8>.

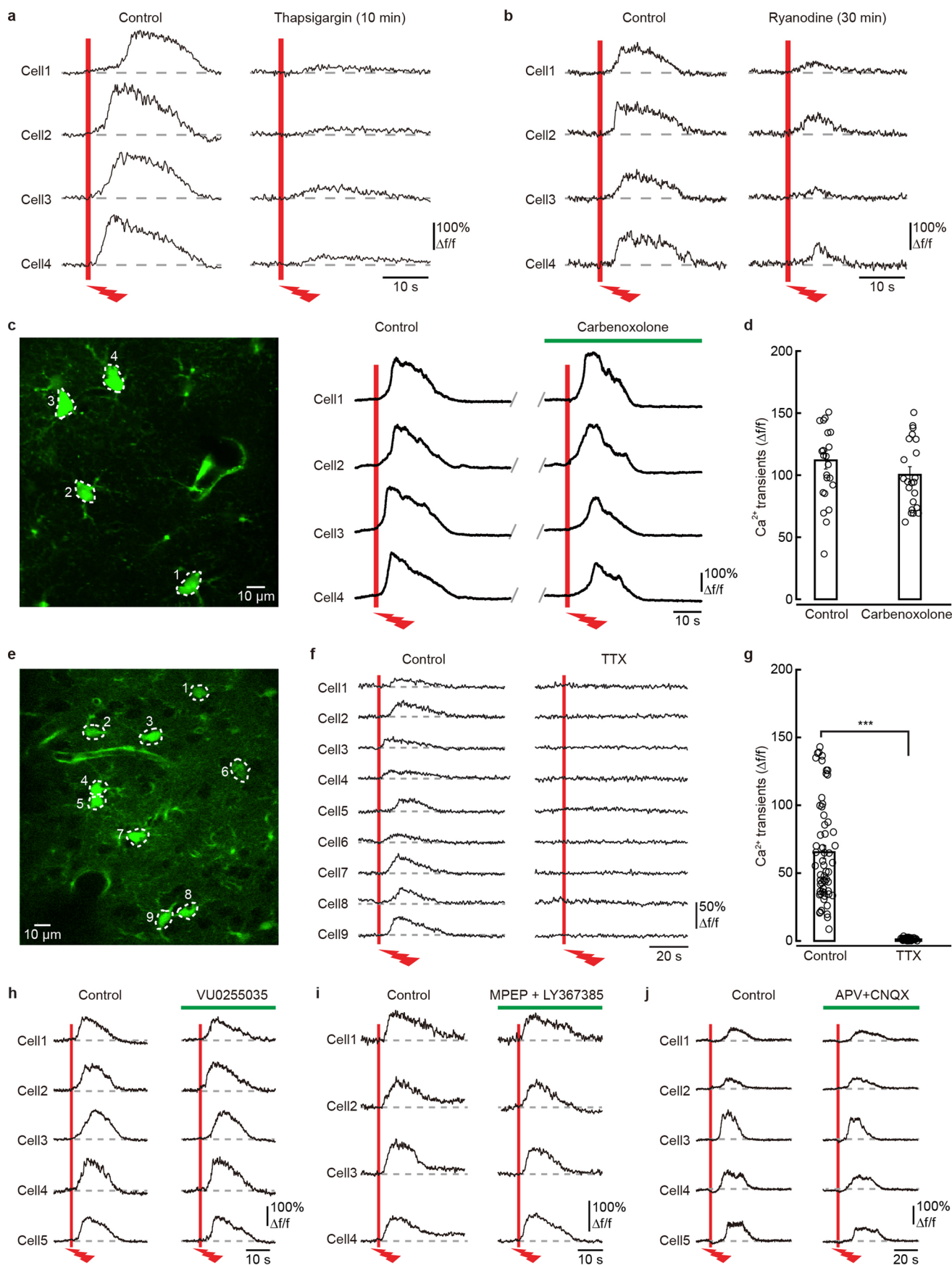
Correspondence and requests for materials should be addressed to Arthur Konnerth or Xiaowei Chen.

Reprints and permissions information is available at www.nature.com/reprints.

Nature Neuroscience thanks Balazs Hangya and the other, anonymous, reviewer(s) for their contribution to the peer review of this work.

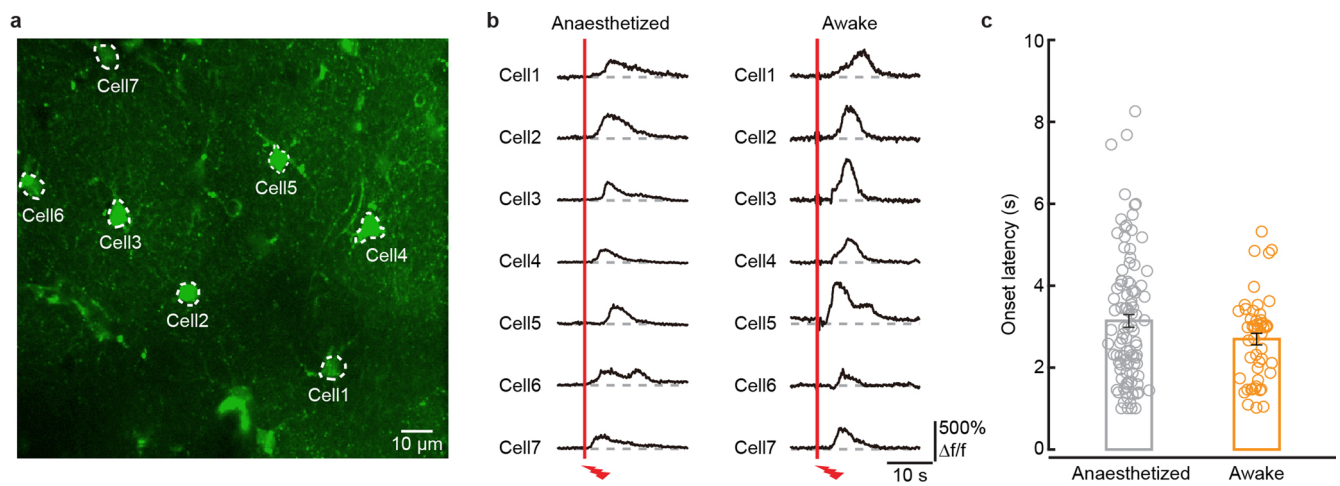


Extended Data Fig. 1 | Sound-evoked Ca^{2+} signals in astrocytes of the mouse auditory cortex. **a**, Two-photon fluorescence image of fluo-8AM-stained astrocytes in layer 2/3 of the mouse auditory cortex. The red arrowhead indicates an astrocyte that responded to sound ('Sound responder'), while grey arrowheads indicate non-responding cells to sound ('Sound non-responders'). **b**, Ca^{2+} traces ($\Delta f/f$) corresponding to the astrocytes indicated in panel a (sound stimuli indicated by grey bars; duration 9.9 s, pure tone of 8 kHz frequency, intensity 70 dB sound pressure level). Astrocytes were defined as 'responders' (Fig. 1 and Extended Data Fig. 1) when the maxima of averaged Ca^{2+} signals from 3 consecutive trials 0–9 s after stimuli were above $3 \times \text{s.d.}$ of baseline. Therefore, the 'non-responders' could include occasional weak responses that were smaller than $3 \times \text{s.d.}$ of baseline traces.

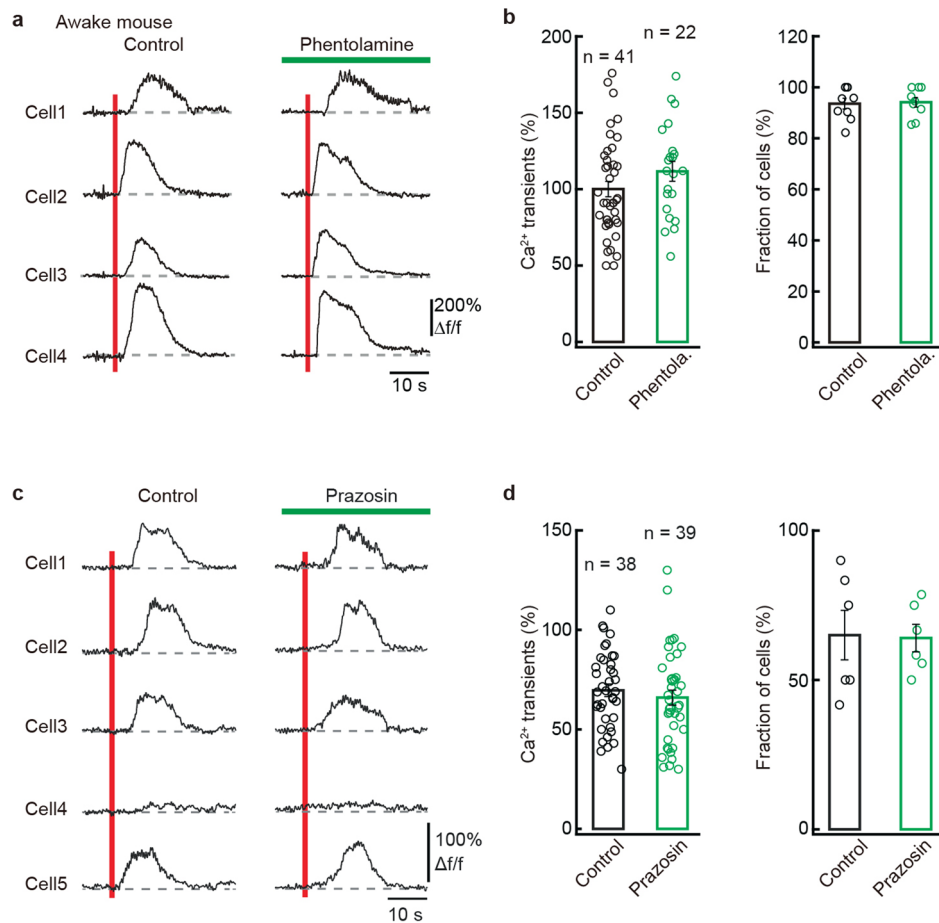


Extended Data Fig. 2 | See next page for caption.

Extended Data Fig. 2 | Footshock-induced astrocytic Ca^{2+} transients involve Ca^{2+} release from internal stores and are blocked by TTX, but not require gap junctions, mAChRs, mGluRs or iGluRs in the adult mouse cortex. **a, b**, Representative cells showing footshock-induced astrocytic Ca^{2+} signals before and after application of thapsigargin (**a**) or ryanodine (**b**). **c**, Footshock-induced Ca^{2+} transients in astrocytes of auditory cortex without or with a gap junction blocker carbenoxolone. Left, two-photon image of fluo-8AM labelled astrocytes. Right, representative footshock-evoked Ca^{2+} transients in astrocytes indicated in the left panel. **d**, Summary results of the carbenoxolone experiments. Note a minor but no significant reduction in the amplitude of footshock-evoked Ca^{2+} transients in the presence of carbenoxolone (control versus carbenoxolone, $Z=1.6499$, $P=0.0990$; $n=25$ cells from 4 mice, two-sided Wilcoxon signed-rank test). **e**, Two-photon image of fluo-8AM-stained astrocytes in layer 2/3 of the mouse auditory cortex. **f**, Footshock-induced Ca^{2+} transients in astrocytes, outlined in panel **a**, before and after local application of TTX ($0.5\ \mu\text{M}$). **g**, Summary of the TTX experiments (control versus TTX, $Z=6.4515$, $P=1.1076\ \text{E}-10$; $***P<0.001$, two-sided Wilcoxon signed-rank test, $n=55$ cells from 5 mice). **h**, Representative cells showing footshock-induced astrocytic Ca^{2+} transients without or with mAChR antagonist VU0255035. **i**, Representative cells showing footshock-induced astrocytic Ca^{2+} transients without or with the combination of group I mGluR antagonists MPEP and LY367385. **j**, Representative cells showing footshock-induced astrocytic Ca^{2+} transients without or with the combination of iGluR (ionotropic glutamate receptor) antagonists APV and CNQX. All data in the figure are shown as mean \pm s.e.m.

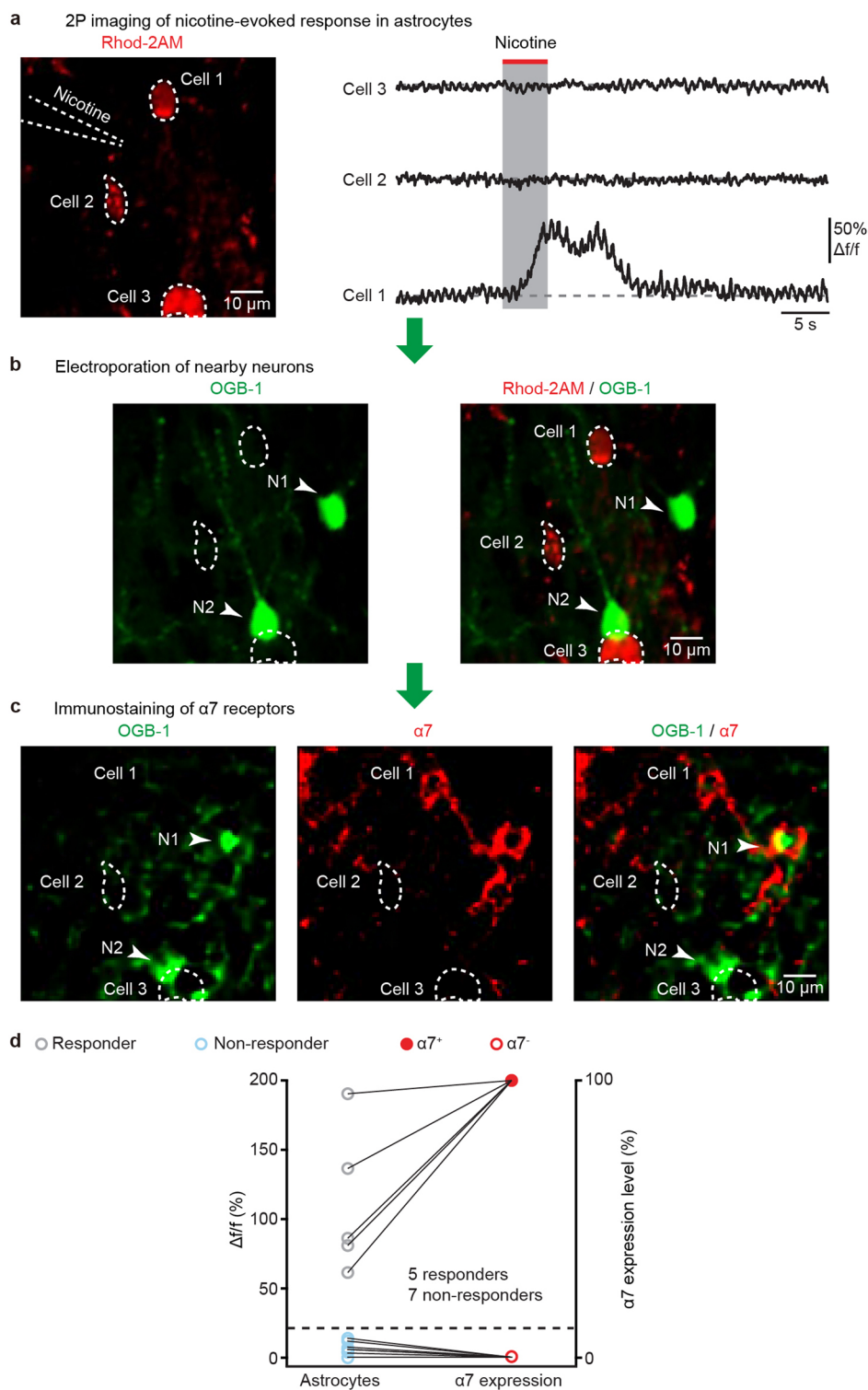


Extended Data Fig. 3 | Footshock stimulation-evoked astrocytic Ca^{2+} signals in the auditory cortex of anaesthetized and awake mice. **a**, Two-photon image of labeled astrocytes in layer 2/3 of the mouse auditory cortex. **b**, Footshock-evoked Ca^{2+} transients ($\Delta f/f$) from the astrocytes indicated in panel **a** in anaesthetized (left) and awake (right) states from the same imaging plane in the same mouse (footshock stimuli indicated by red dashed boxes). Awake recordings were achieved at least 1 hour after stopping isoflurane application. **c**, Bar graphs summarizing the onset latencies of astrocytic Ca^{2+} transients during anaesthetized and awake states. $n=101$ cells from 5 mice in the anaesthetized group; $n=51$ cells from 4 mice in the awake group (anaesthetized versus awake, $Z=1.2097$, $P=0.2264$, two-sided Wilcoxon rank-sum test). All data in the figure are shown as mean \pm s.e.m.

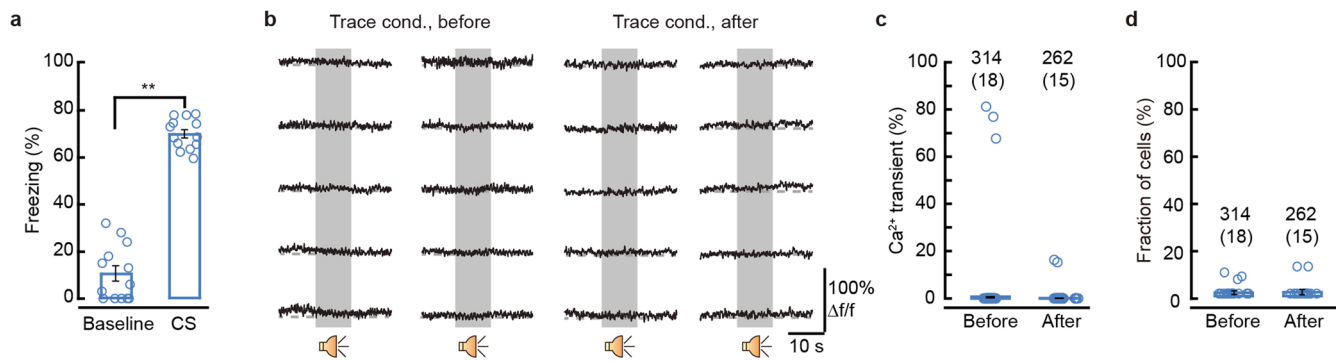


Extended Data Fig. 4 | Neither α -adrenergic receptors nor α 1-adrenergic receptors are required for footshock-induced astrocytic Ca^{2+} transients.

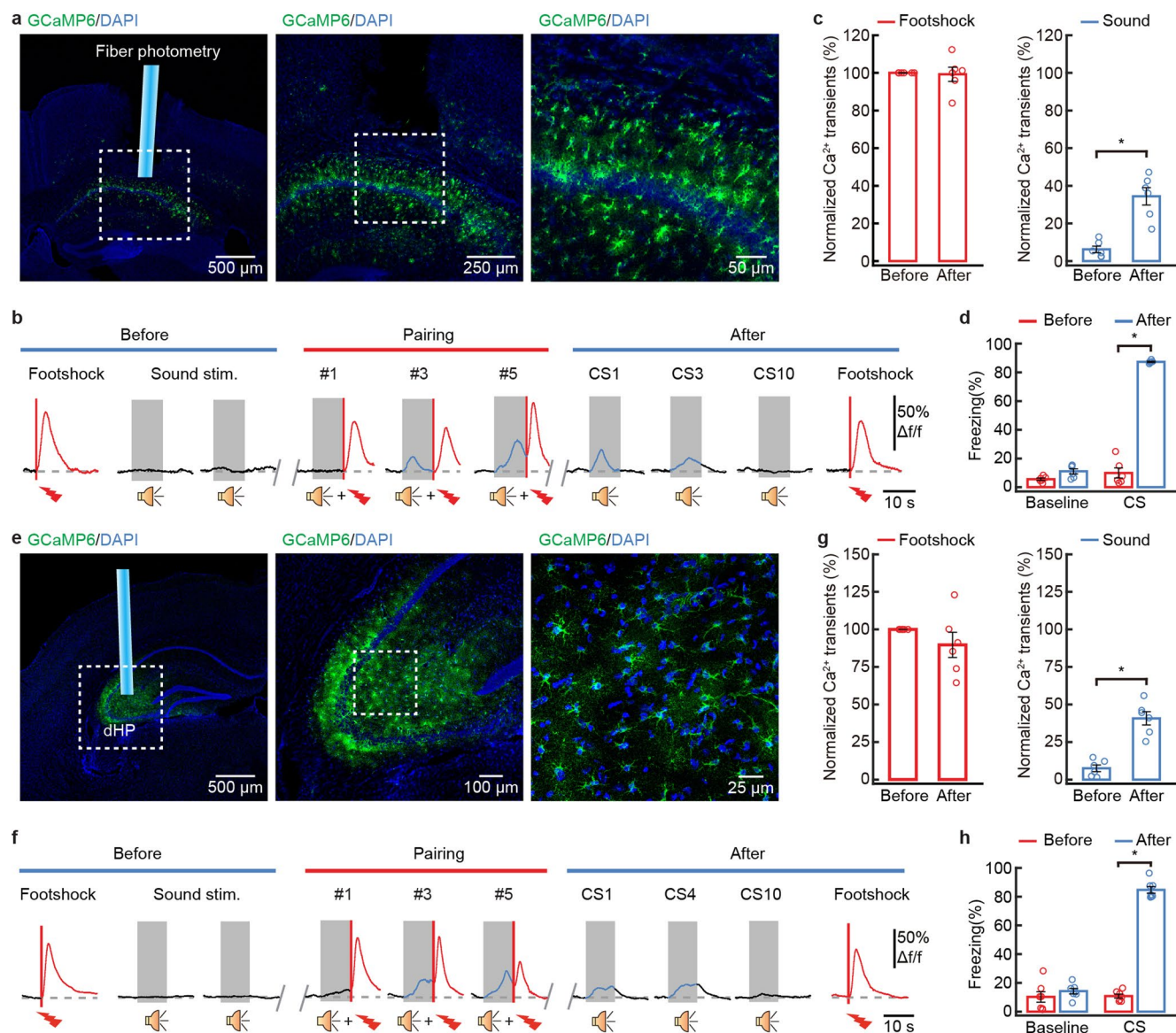
a, Representative cells showing footshock-induced astrocytic Ca^{2+} transients without or with the α -adrenergic receptor antagonist phentolamine. **b**, Summary of the amplitudes of footshock-evoked astrocytic responses and the fractions of responding cells in the presence of phentolamine. No significant effect was observed (left panel: the number of cells tested is indicated on the top of each bar. Data are from 3 mice; control versus phentolamine, $Z = -1.4206$, $P = 0.1554$; right panel: $n = 9$ fields of view, 41 cells from 3 mice, $n = 9$ fields of view, 22 cells from 3 mice; control versus Phentolamine, $Z = -0.1349$, $P = 0.8927$; two-sided Wilcoxon rank-sum test). All recordings in this figure were performed in the auditory cortex of head-fixed, awake mice. **c**, Footshock-induced astrocytic Ca^{2+} transients without or with the α -1 adrenergic receptor antagonist prazosin in 5 representative cells. **d**, Summary of the amplitudes of footshock-evoked astrocytic responses and the fractions of responding cells in the presence of prazosin. No significant effect was observed (left panel: the number of cells is indicated in each bar graph. Data are from 4 mice; control versus prazosin, $Z = 0.7183$, $P = 0.4725$; right panel: $n = 6$ fields of view, 64 cells from 4 mice in control group; $n = 6$ fields of view, 62 cells from 4 mice in prazosin group; control versus prazosin, $Z = 0.0000$, $P = 1.0000$; two-sided Wilcoxon rank-sum test). All recordings in this figure were performed in the auditory cortex. All data in the figure are shown as mean \pm s.e.m.



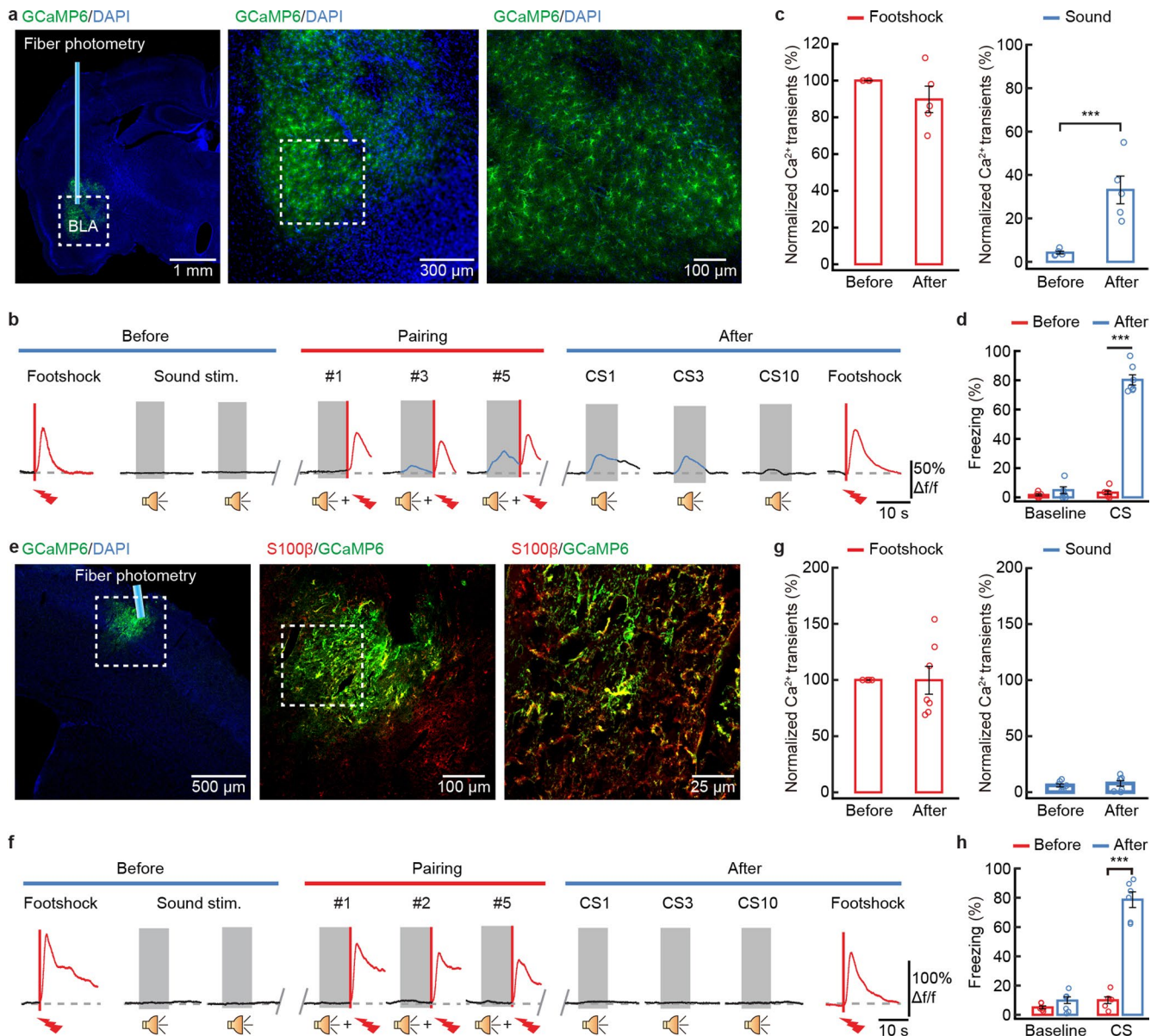
Extended Data Fig. 5 | Specific expression $\alpha 7$ -nicotinic receptors in those astrocytes that respond to nicotine application. **a**, *In vivo* two-photon imaging of astrocyte response to local nicotine application. Left, an imaging plane showing 3 astrocytes labelled with rhod-2AM. The dashed lines indicate the position of an electrode for nicotine application. Right, nicotine-evoked astrocytic Ca^{2+} transient in cell1 but not in cell2 and cell3. **b**, Electroporation of two nearby neurons (N1 and N2) in the same imaging plane with OGB-1 (green) as markers. Left, green channel showing OGB-1-labeled neurons. Right, red and green channels showing both rhod-2 AM-labeled astrocytes and OGB-1-labeled neurons. **c**, Immunostaining of $\alpha 7$ receptors. Post-hoc histology was performed after *in vivo* two-photon imaging. Note the expression of $\alpha 7$ receptors in cell1 but not in cell2 and cell3, consistent with the *in vivo* two-photon imaging result. **d**, Summary of all astrocytes tested, showing that 5 astrocytes responding to nicotine (responder) also express $\alpha 7$ receptors, while 7 non-responders express no $\alpha 7$ receptors. These experiments were repeated in 3 mice.



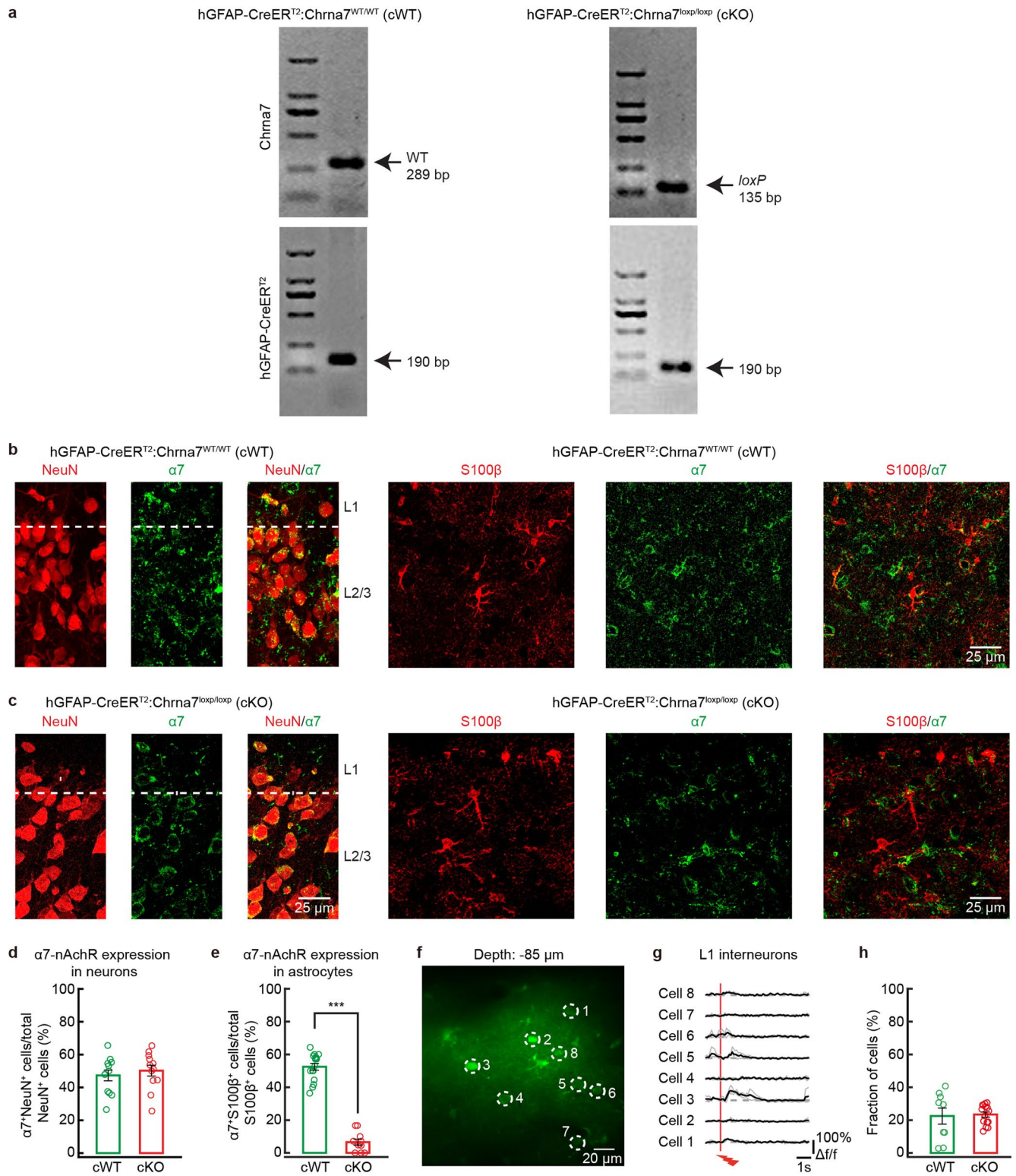
Extended Data Fig. 6 | Absence of sound-evoked astrocytic Ca²⁺ signals following trace fear conditioning. **a**, Summary of the freezing levels after trace fear conditioning ($n=13$ mice; baseline versus CS⁺, $Z=-3.1798$, $P=0.0015$, two-sided Wilcoxon signed rank test, $**P<0.01$). **b**, Ca²⁺ traces from astrocytes that were not responsive to sound stimulation before (left) and after (right) trace fear conditioning (black traces: two consecutive sound stimuli). **c**, Bar graph summarizing of the amplitude of astrocytic Ca²⁺ transients in response to sound stimulation before and after trace fear conditioning. Data of 'before' group is the same as the 'control' group in Fig. 6i. The numbers of cells (and mice) are indicated in each bar graph (before versus after, $Z=0.2550$, $P=0.7987$, Two-sided Wilcoxon rank-sum test). **d**, Bar graph summarizing of the fraction of astrocytes responding to sound stimulation before and after trace fear conditioning (before: $1.42 \pm 0.78\%$, after: $1.67 \pm 1.14\%$; before versus after, $Z=0.058$, $P=0.9538$, Two-sided Wilcoxon rank-sum test). Data of 'before' group is the sum of the 'control' group in Fig. 6i. The numbers of cells (and mice) are indicated in each bar graph. For this trace fear conditioning experiment, the trace interval separating CS⁺ and US was 20 s. Five pairings were delivered for conditioning and the interval between two pairings was 3 min. All data in the figure are shown as mean \pm s.e.m.



Extended Data Fig. 7 | De novo induction of sound-evoked astrocytic Ca^{2+} responses by fear conditioning in the hippocampus (CA1 and dorsal hippocampus, dHP). **a**, Confocal images of astrocytes labeled by AAV5-GfaABC₁D-cytoGCaMP6f-SV40 (green) in the CA1 region. **b**, Astrocytic Ca^{2+} transients in response to footshock or sound before, during and after pairing in the CA1 region. **c**, Bar graphs summarizing the amplitudes of astrocytic Ca^{2+} transients in response to footshock (left) or sound (right) before and after conditioning in the CA1 region. $n=6$ mice (left, footshock: before versus after, $Z=0.1348$, $P=0.8927$; right, sound: before versus after, $Z=-2.2014$, $P=0.0277$; $*P<0.05$, two-sided Wilcoxon signed rank test). **d**, Summary of the freezing levels before and after fear conditioning. $n=6$ mice (baseline: before versus after, $Z=-0.9439$, $P=0.3452$; CS: before versus after, $Z=-2.2014$, $P=0.0277$; $*P<0.05$, two-sided Wilcoxon signed rank test). **e**, Confocal images of astrocytes labeled by AAV5-GfaABC₁D-cytoGCaMP6f-SV40 (green) in the dHP. **f**, Astrocytic Ca^{2+} transients in response to footshock or sound before, during and after pairing in the dHP. **g**, Bar graphs summarizing the amplitudes of astrocytic Ca^{2+} transients in response to footshock (left) or sound (right) before and after conditioning in the dHP. $n=6$ mice (left, footshock: before versus after, $Z=1.1531$, $P=0.2489$; right, sound: before versus after, $Z=-2.2014$, $P=0.0277$; $*P<0.05$, two-sided Wilcoxon signed rank test). **h**, Summary of the freezing levels before and after fear conditioning. $n=7$ mice (baseline: before versus after, $Z=-0.8452$, $P=0.3980$; CS: before versus after, $Z=-2.3664$, $P=0.0180$; $*P<0.05$, two-sided Wilcoxon signed rank test). All data in the figure are shown as mean \pm s.e.m.



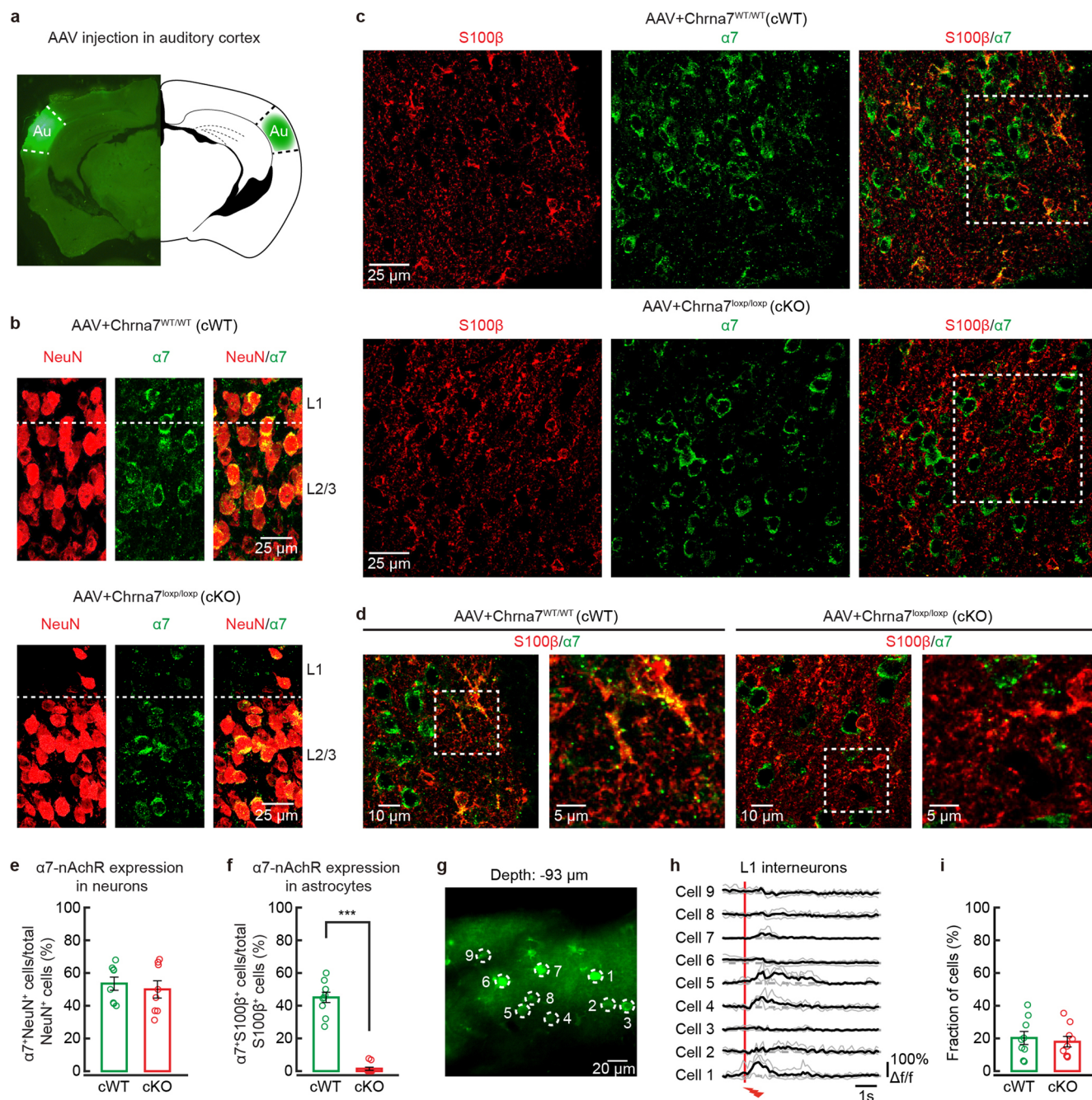
Extended Data Fig. 8 | De novo induction of sound-evoked Ca^{2+} astrocytic responses by fear conditioning in the basolateral amygdala (BLA), but not in the somatosensory cortex. **a**, Confocal images of astrocytes labeled by AAV5-GfAP6f-SV40 (green) in the BLA. **b**, Astrocytic Ca^{2+} transients in response to footshock or sound before, during and after pairing in the BLA of amygdala. **c**, Bar graphs summarizing the amplitudes of astrocytic Ca^{2+} transients in response to footshock (left) or sound (right) before and after conditioning in the BLA. $n = 5$ mice (left, footshock: before versus after, $Z = 1.4832$, $P = 0.1380$; right, sound: before versus after, $Z = -2.0226$, $P = 0.0431$; $*P < 0.05$, two-sided Wilcoxon signed rank test). **d**, Summary of the freezing levels before and after fear conditioning. $n = 7$ mice (baseline: before versus after, $Z = -1.5724$, $P = 0.1159$; CS: before versus after, $Z = -2.3664$, $P = 0.0180$; $*P < 0.05$, two-sided Wilcoxon signed rank test). **e**, Confocal imaging of astrocytes labeled by AAV5-GfAP6f-SV40 (green) and S100 β (red) in the somatosensory cortex. **f**, Astrocytic Ca^{2+} transients in response to footshock or sound before, during and after pairing in the somatosensory cortex. **g**, Bar graphs summarizing the amplitudes of astrocytic Ca^{2+} transients in response to footshock (left) or sound (right) before and after conditioning in the somatosensory cortex. $n = 7$ mice (left, footshock: before versus after, $Z = 0.1690$, $P = 0.8658$; right, sound: before versus after, $Z = -1.0142$, $P = 0.3105$; two-sided Wilcoxon signed rank test). **h**, Summary of the freezing levels before and after fear conditioning. $n = 6$ mice (baseline: before versus after, $Z = -1.5724$, $P = 0.1159$; CS: before versus after, $Z = -2.2014$, $P = 0.0277$; $*P < 0.05$, two-sided Wilcoxon signed rank test). All data in the figure are shown as mean \pm s.e.m.



Extended Data Fig. 9 | See next page for caption.

Extended Data Fig. 9 | Characterization of tamoxifen-inducible astrocytic $\alpha 7$ -nAChR conditional knockout mice (hGFAP-CreER^{T2}/*Chrna7*^{loxp/loxp}, cKO).

a, PCR analysis of hGFAP-CreER^{T2}:*Chrna7*^{WT/WT} (cWT) and hGFAP-CreER^{T2}:*Chrna7*^{loxp/loxp} mice ($\alpha 7$ -cKO mice). The experiment was repeated before immunostaining and two-photon imaging experiment. **b, c**, $\alpha 7$ -nAChR immunostaining in the auditory cortex of a cWT (**b**) or a cKO (**c**) mouse indicates a pronounced loss of $\alpha 7$ -nAChR-positive astrocytes in cKO. Left, neuronal staining (neuronal marker: NeuN) in L1 and L2/3 in the auditory cortex. Right, astrocyte staining (astrocyte marker: S100 β) in the auditory cortex. One astrocyte from panel **b** was shown in Fig. 7b in an expanded scale. **d**, Bar graphs summarizing the $\alpha 7$ -nAChR expression in neurons in the auditory cortex of cWT and cKO mice. $n = 12$ sections from 4 mice in each group (cWT versus cKO, $Z = -0.6067$, $P = 0.5440$, two-sided Wilcoxon rank-sum test). **e**, Bar graphs summarizing the $\alpha 7$ -nAChR expression in astrocytes in the auditory cortex of cWT and cKO mice. $n = 16$ sections from 5 mice in cWT group; $n = 11$ sections from 4 mice in cKO group. (cWT versus cKO, $Z = 4.3257$, $P = 1.52 \times 10^{-5}$, $***P < 0.001$, two-sided Wilcoxon rank-sum test). **f**, *In vivo* two-photon Ca²⁺ imaging of L1 interneurons in the auditory cortex of a cKO mouse, with dashed lines indicating neurons of interest. **g**, Single trials and their average of Ca²⁺ responses to footshock from these neurons as indicated in panel **f**. **h**, Bar graph summarizing the fraction of L1 neurons that responded to footshock in cWT and cKO mice. $n = 9$ fields of view, 42 cells from 3 mice in cWT group; $n = 15$ fields of view, 127 cells from 6 mice in cKO group (cWT versus cKO, $Z = 0.2684$, $P = 0.7884$; two-sided Wilcoxon rank-sum test). All data in the figure are shown as mean \pm s.e.m.



Extended Data Fig. 10 | Characterization of virus-induced region-specific astrocytic $\alpha 7$ -nAChR conditional knockout mice (AAV + *Chrna7*^{loxP/loxP}, cKO). **a**, Post-hoc image showing the position of AAV-transfected region in the extended auditory cortex. **b**, Neuron (NeuN) and $\alpha 7$ -nAChR staining in L1 and L2/3 in the auditory cortex of a cWT (upper; AAV5-GfaABC₁D-Cre was injected into the auditory cortex of *Chrna7*^{WT/WT} mice) or a cKO (lower; AAV5-GfaABC₁D-Cre was injected into the auditory cortex of *Chrna7*^{loxP/loxP} mice) mouse. **c**, $\alpha 7$ -nAChR and S100 β immunostaining in the auditory cortex of a cWT (upper) or a cKO (lower) mouse, indicating a pronounced loss of $\alpha 7$ -nAChR-positive astrocytes in cKO. **d**, High-magnification images showing immunostaining of $\alpha 7$ -nAChRs and S100 β in cWT (left) and cKO (right) as indicated by the white boxes in panel **c**. **e**, Bar graphs summarizing the $\alpha 7$ -nAChR expression in neurons in the auditory cortex of cWT and cKO mice. $n = 8$ sections from 4 mice in each group (cWT versus cKO, $Z = 0.3153$, $P = 0.7525$, two-sided Wilcoxon rank-sum test). **f**, Bar graphs summarizing the $\alpha 7$ -nAChR expression in astrocytes in the auditory cortex of cWT and cKO mice. $n = 10$ sections from 4 mice in each group. (cWT versus cKO, $Z = 3.8675$, $P = 1.10 \text{ E-}4$, *** $P < 0.001$, two-sided Wilcoxon rank-sum test). **g**, In vivo two-photon Ca^{2+} imaging of L1 interneurons in the auditory cortex of an AAV-induced cKO mouse, with dashed lines indicating neurons of interest. **h**, Single trials and their average of Ca^{2+} responses to footshock from these neurons as indicated in panel **g**. **i**, Bar graph summarizing the fraction of L1 neurons that responded to footshock in cWT and cKO mice. $n = 9$ fields of view, 45 cells from 3 mice in cWT group; $n = 9$ fields of view, 52 cells from 3 mice in cKO group (cWT versus cKO, $Z = 0.1766$, $P = 0.8598$, two-sided Wilcoxon rank-sum test). All data in the figure are shown as mean \pm s.e.m.

Reporting Summary

Nature Research wishes to improve the reproducibility of the work that we publish. This form provides structure for consistency and transparency in reporting. For further information on Nature Research policies, see our [Editorial Policies](#) and the [Editorial Policy Checklist](#).

Statistics

For all statistical analyses, confirm that the following items are present in the figure legend, table legend, main text, or Methods section.

- | | |
|-----|-----------|
| n/a | Confirmed |
|-----|-----------|
- The exact sample size (n) for each experimental group/condition, given as a discrete number and unit of measurement
 - A statement on whether measurements were taken from distinct samples or whether the same sample was measured repeatedly
 - The statistical test(s) used AND whether they are one- or two-sided
Only common tests should be described solely by name; describe more complex techniques in the Methods section.
 - A description of all covariates tested
 - A description of any assumptions or corrections, such as tests of normality and adjustment for multiple comparisons
 - A full description of the statistical parameters including central tendency (e.g. means) or other basic estimates (e.g. regression coefficient) AND variation (e.g. standard deviation) or associated estimates of uncertainty (e.g. confidence intervals)
 - For null hypothesis testing, the test statistic (e.g. F , t , r) with confidence intervals, effect sizes, degrees of freedom and P value noted
Give P values as exact values whenever suitable.
 - For Bayesian analysis, information on the choice of priors and Markov chain Monte Carlo settings
 - For hierarchical and complex designs, identification of the appropriate level for tests and full reporting of outcomes
 - Estimates of effect sizes (e.g. Cohen's d , Pearson's r), indicating how they were calculated

Our web collection on [statistics for biologists](#) contains articles on many of the points above.

Software and code

Policy information about [availability of computer code](#)

Data collection Electrophysiological data were collected by PatchMaster v2x65 (HEKA Elektronik); Two-photon imaging data and fiber recording data were collected by custom software written in LabVIEW 2014 (National Instruments). Confocal imaging data were collected by LAS X; Immunoelectron microscopy data were collected by a JEM-1400 electron microscope (JEOL, Tokyo, Japan) equipped with a CCD camera (Olympus VELETA, Tokyo, Japan) and its application software (ITEM-EMSYS).

Data analysis ImageJ 1.51 was used for image processing; Two photon imaging data and fiber recording data were first processed by LabVIEW 2014 (National Instruments) and then analyzed by Igor Pro 5.0 (Wavemetrics); Video analyses and Statistical tests were performed by MATLAB 2014a (Math Works).

For manuscripts utilizing custom algorithms or software that are central to the research but not yet described in published literature, software must be made available to editors and reviewers. We strongly encourage code deposition in a community repository (e.g. GitHub). See the Nature Research [guidelines for submitting code & software](#) for further information.

Data

Policy information about [availability of data](#)

All manuscripts must include a [data availability statement](#). This statement should provide the following information, where applicable:

- Accession codes, unique identifiers, or web links for publicly available datasets
- A list of figures that have associated raw data
- A description of any restrictions on data availability

No data sets that require mandatory deposition into a public database were generated during the current study. Any data generated and/or analyzed during the current study are available from the corresponding author on reasonable request. Source data underlying Figs. 1–8 and Extended Data Figs. 2–4, 6–10 and Supplementary Figs. 5–6 are available as a Source data file.

Field-specific reporting

Please select the one below that is the best fit for your research. If you are not sure, read the appropriate sections before making your selection.

Life sciences Behavioural & social sciences Ecological, evolutionary & environmental sciences

For a reference copy of the document with all sections, see [nature.com/documents/nr-reporting-summary-flat.pdf](https://www.nature.com/documents/nr-reporting-summary-flat.pdf)

Life sciences study design

All studies must disclose on these points even when the disclosure is negative.

Sample size	No statistical methods were used to pre-determine sample sizes. Samples sizes were determined based on our own previous studies about using behavioral, optical imaging and electrophysiological recording approaches (Zhang et al, Cerebral Cortex, 2016; Yao et al, Nature Neuroscience; Qin et al, Neuron). Samples sizes adopted in this study were sufficient for detecting robust effect.
Data exclusions	For optical fiber-based Ca ²⁺ recordings, any mice whose virus injection sites or fiber tip sites were missed were excluded from data analysis.
Replication	Experiments were repeated multiple times on independent occasions as indicated in the Methods and/or Figure legends. All attempts at replication were successful.
Randomization	For all experiments, samples were randomized where appropriate for data collection and analysis.
Blinding	In the studies, investigators were blinded to groups for data collection and processing.

Reporting for specific materials, systems and methods

We require information from authors about some types of materials, experimental systems and methods used in many studies. Here, indicate whether each material, system or method listed is relevant to your study. If you are not sure if a list item applies to your research, read the appropriate section before selecting a response.

Materials & experimental systems

Methods

n/a	Involved in the study	n/a	Involved in the study
<input type="checkbox"/>	<input checked="" type="checkbox"/> Antibodies	<input checked="" type="checkbox"/>	<input type="checkbox"/> ChIP-seq
<input checked="" type="checkbox"/>	<input type="checkbox"/> Eukaryotic cell lines	<input checked="" type="checkbox"/>	<input type="checkbox"/> Flow cytometry
<input checked="" type="checkbox"/>	<input type="checkbox"/> Palaeontology and archaeology	<input checked="" type="checkbox"/>	<input type="checkbox"/> MRI-based neuroimaging
<input type="checkbox"/>	<input checked="" type="checkbox"/> Animals and other organisms		
<input checked="" type="checkbox"/>	<input type="checkbox"/> Human research participants		
<input checked="" type="checkbox"/>	<input type="checkbox"/> Clinical data		
<input checked="" type="checkbox"/>	<input type="checkbox"/> Dual use research of concern		

Antibodies

Antibodies used	Goat anti-GFAP, Abcam, Cat#Ab53554; Rabbit anti-NeuN, Abcam, Cat#Ab177487; Mouse anti- α 7-nAChR, Sigma, Cat#M220; Rabbit anti-S100 β , Synaptic Systems, Cat#287003; Chicken anti-GFP, Abcam, Cat# Ab13970; Donkey anti-goat (Alexa Fluor 594), Invitrogen, Cat# A-11058; Donkey anti-rabbit (Alexa Fluor 594), Invitrogen, Cat# A-21207; Donkey anti-mouse (Alexa Fluor 488), Invitrogen, Cat# A-21202; Donkey anti-chicken (Alexa Fluor 488), Jackson ImmunoResearch Labs, Cat#703-545-155; Donkey anti-goat (Alexa Fluor 488), Jackson ImmunoResearch Labs, Cat#705-545-003; Nanogold-IgG Goat anti-mouse IgG antibody (Nanoprobes, 2001, 1:100, Yaphank, New York USA); Biotin-SP conjugated donkey anti-rabbit IgG antibody (Merck Millipore, AP182B, 1:200, Darmstadt, Hessen, Germany)
Validation	Goat anti-GFAP: IHC-FrFl, WB, IHC-P, IHC-Fr, IHC-FoFr, ICC/IF, reacts with: Mouse, Rat, Human; Rabbit anti-NeuN: Flow Cyt, ICC/IF, IHC-FoFr, IHC-Fr, IHC-P, mIHC, WB, reacts with: Mouse, Rat, Sheep, Goat, Cat, Dog, Human, Zebrafish, Common marmoset; α 7-nAChR: immunohistochemistry (frozen sections), react with: Mouse, Human (denatured), Rat (denatured), Chicken; Rabbit anti-S100 β : WB, IP, ICC, IHC, IHC-P/FFPE, react with: Mouse, Rat; Chicken anti-GFP: IHC-P, WB, IHC - Wholemount, IHC-FrFl, ICC/IF, IHC-Fr, IHC-FoFr, react with: Species independent.

Animals and other organisms

Policy information about [studies involving animals](#); [ARRIVE guidelines](#) recommended for reporting animal research

Laboratory animals	C57BL/6 mice were obtained from Laboratory Animal Center at the Third Military Medical University. C57BL/6N-Chrna7tm1a(EUCOMM)Hmgu/H (EM#07778) mice were obtained from European Mouse Mutant Archive. B6.Cg-Tg(hGFAP-Cre/ERT2)505Fmv/J (JAX#012849) and B6.Cg-Gt(ROSA)26Sortm14(CAG-tdTomato)Hze/J (JAX#007914) mice were ordered from Jackson
--------------------	---

Laboratories. Male, 8-12-week-old mice were used in the present study. Mice were housed on a 12-h light/dark cycle, at 22-25 °C and in 50-60% relative humidity with ad libitum access to food and water.

Wild animals

No wild animals were used in this study.

Field-collected samples

No field-collected samples were used in this study.

Ethics oversight

Third Military Medical University Animal Care and Use Committee; German animal welfare act and protocols approved by the government of Bavaria, Germany

Note that full information on the approval of the study protocol must also be provided in the manuscript.